LOW-VELOCITY IMPACT DAMAGE AND ITS PROPAGATION UNDER COMPRESSIVE LOAD IN CURVED, GRAPHITE/EPOXY PANELS

Thesis by

Tony Magaldi

In Partial Fulfillment of the Requirements

for the Degree of

Aeronautical Engineer

California Institute of Technology

Pasadena, California

1983

(Submitted August 1982)

ACKNOWLEDGEMENTS

I especially would like to express my appreciation to my advisor, Professor C.D. Babcock, for his guidance, support, and patience. I also wish to gratefully acknowledge Professor W.G. Knauss for his support.

Many thanks and best wishes to all my friends in the Solid Mechanics group at GALCIT and Herzl Chai in particular for his assistance in the laboratory. Special thanks go also to Ms. M. Nyiri for her help preparing this manuscript. In addition my thanks go to Mr. H. Hamaguchi, Mrs. B. Wood, and all the members of the Aeronautics Machine and Electronics shops for their help.

I would also like to extend my thanks to NASA for their support of this project and to Boeing Co. for manufacturing the Graphite/Epoxy plates.

This work is dedicated to Mom and Dad.

TABLE OF CONTENTS

NOMENCLATURE

a	Amplitude of initial imperfection function
b	Panel width
b_i	Initial delamination diameter (in.)
E	Young's modulus (psi)
F	Defined by eqn. (3.11)
f	Fringe constant
G	Energy release rate
h_1,h_2	Distance between moiré grating and specimen
h_d	Delamination length (height) in direction of applied load
i	Angle of incidence
kV	Kilovolt
l	Panel length
P	Moiré grating pitch
R	Panel radius
S	Defined by eqn. (3.10)
SX-n	Small panel test designation
t	Thickness
V	Impact velocity
V_P	Delamination propagation velocity
u,v,w	Displacement components
w_d	Delamination width
x,y,z	Coordinate axes
X-n	Large panel test designation
α	Moiré observation angle
β	Circumferential panel angle
Γ_o	Fracture energy

δ_d	Amplitude of delamination buckle
Δt	Camera timescale
ϑ	Curvature parameter
λ	Normalized load parameter (σ / E)
λ_{cr}	Critical buckling load
λ_{fl}	Buckling load for flat plate
λ_μ	Normalized buckling load for panel with imperfection
λ^*	Defined by eqn. (3.15)
μ	Nondimensional imperfection parameter
μf	Microfarad
ν	Poisson's ratio
σ	Stress

TERMINOLOGY

C-scan	Non destructive, ultrasonic inspection technique
delamination	The separation of the layers of material in a laminate
Gr/Ep	Graphite/epoxy
ILS	Interlaminar shear
interlaminar	Descriptive term pertaining to some object or event occurring between two adjacent laminae
lamina	A single layer of unidirectional composite material
laminate	Material composed of several layers
lpi	Lines per inch
matrix	The essentially homogeneous material in which the fibers or filaments of a composite are embedded
OBS	Oblique-shadow moiré
pre-preg	Raw materials for composites consisting of a combination of filaments and a matrix
threshold curve	Survivability or damage tolerance curve for laminates impacted while under load

LIST OF FIGURES

ABSTRACT

An experimental study was conducted to investigate the influence of plate curvature on low-velocity impact damage and its propagation under compressive load in thick, Graphite/Epoxy laminates. High-speed photography coupled with the oblique-shadow moiré technique indicates that initial impact damage and its subsequent propagation through delamination buckling act as separate mechanisms during the catastrophic failure process.

Results of an initial-postbuckling analysis for the buckling of thin cylindrical plates in axial compression were used to assess the effect of plate curvature on the conditions necessary for delamination buckling. Although curvature was found to increase the buckling load at the expense of a greater imperfection sensitivity, the effect is insignificant in thin shells if the plate width (i.e. initial delamination width) is small compared to the plate's radius.

When compared with the experimental and analytic findings of similar studies involving flat Gr/Ep laminates, results reveal that the 15 inch plate radius used for this series of experiments had a negligible influence on the inital damage and delamination propagation mechanisms.

CHAPTER 1 - INTRODUCTION

In recent years advanced composite materials have seen increasing use in structures where reduced weight can justify high material and manufacturing costs. Graphite/Epoxy (Gr/Ep), perhaps the most widely used high-stiffness composite, is the subject of the experimental and analytic studies of this report. Gr/Ep lamina consist of small diameter (25 microns), high modulus (E_x = 19x10^6 PSI) fibers unidirectionally embedded in an epoxy matrix. While the filaments are the primary load-carrying element, the matrix stabilizes the fibers in compression, loads and unloads the filaments by shear and generally provides the transverse properties. Each layer is highly anisotropic, and laminate properties are determined by the number of layers and their orientation. Although material homogeneity is usually assumed for structural analysis, the actual inhomogeneities clearly characterize the many failure modes of this material. For the most part, it has been observed that while tensile failures are associated with fiber fracture, compression and shear failures of the material often propagate through the matrix and/or along the fiber/matrix interface.

In addition to the weight saving advantage, laminate construction permits material tailoring (i.e. preferential orientation of lamina) to accommodate specific load conditions and/or environments. Unlike conventional aircraft materials, however, Gr/Ep demonstrates nearly linear elastic properties until failure. Without plasticity, there is a poor redistribution of stress around a damaged area (Note: This is a major reason why conventional riveting techniques seriously degrade the strength of composite structures). Also, the brittle nature of the material makes it particularly susceptible to foreign object damage. As a result most of the advanced composite utilization is limited to internal structure or secondary structure (i.e. stiffness requirements usually dictate design).

Before improvements in the damage tolerance of composites can be made, better analytic failure techniques must be developed to establish the material properties and scenarios that affect laminate damage tolerance. This thesis investigates the problem of simultaneous in-plane compression and low-velocity impact in curved Gr/Ep panels.

A common method of investigating the response to impact involves impacting various specimens with projectiles. Post-mortem examinations of Gr/Ep laminates reveal that low-velocity damage includes spallation, intraply and interply cracking. At higher speeds fiber fracture may be accompanied by projectile penetration of the specimen. Ballistic impact damage has been found to be limited to a small area (on order of the size of the projectile) in the vicinity of the impact location. Test results[1] show that matrix properties very significantly affect the energy absorbing ability of composites, and low matrix fracture energies are often associated with unarrested failure propagation. Those epoxies with higher fracture energies consistently demonstrate greater damage tolerance.

Some of the first efforts[2] attempting analytic evaluation of impact damage tried to approximate the local areas of reduced stiffness with simplified damage geometries such as holes. While comparable strength reductions have been achieved, the parametric representations formulated fail to adequately predict the conditions under which the damage will begin to spread. For lack of a better analysis, "open hole" strengths are still used today when designing composite structures. Since this condition may be considered accurate for only a few applications, the effect is merely to put a factor of safety on the associated material properties.

---

1. Byers, B., ref. 3
2. Starnes, J. et al., ref. 13

A more detailed investigation of the influence of this type of damage considers the load conditions (compression in this case) and utilizes high-speed photography and post-mortem examinations to identify the sequence and timescales of the failure mechanisms involved. Because large amounts of energy released during catastrophic failure can complicate the situation, ballistic shots are often taken at low strain levels to isolate the local failure from global plate response.

Observations of the failure of Gr/Ep laminates[3] resulting from low-velocity impact while under compressive load have identified the catastrophic failure process as consisting of two separate phases - impact-induced delamination followed by delamination buckling and propagation. Initial interlaminar separation has been found to occur on a very short timescale (less than 25 μsec) while the subsequent damage propagation leading to global plate failure happens on a millisecond timescale. The second phase is of primary interest when studying ways to control damage growth, and a recent analytic study by Chai[4] has met with some success in describing this failure mechanism in flat panels. Some of the results pertinent to the current experiments are briefly summarized here.

In order to characterize the dominant phenomenon, several problems with varying degrees of simplification were studied. All cases assume quasistatic conditions for growth of the damage under load and utilize large-deflection plate theory as well as fracture mechanics criteria. To represent the layered character of composites, delamination propagation is confined to its own plane, and for analytic simplicity the material properties of the plate are assumed homogeneous, isotropic and linear elastic.

In the simplest case the "thin film" model considers a one-dimensional thin

3. Knauss, W. et al., ref. 6; Chai, H., ref. 4
4. Chai, H., ref. 4

delamination in an infinitely thick plate. A displacement function of unknown amplitude in agreement with clamped boundary conditions is found for the buckled delamination. By considering the overall end shortening of the infinitely thick plate, a closed form solution for the amplitude of the deflection shape can be determined. Knowledge of this deformation allows one to find the stored energy in the buckled layer. Next the change in the stored energy of the system is calculated for the condition that the length of the delamination is incremental increased. Taking the limit of this length increase permits one to calculate the energy release rate, G, for the extending delamination. Comparing this with the fracture energy required to produce a unit of new surface, Γ_o, allows one to describe the conditions for growth and the growth behavior of the "damaged area". Results indicate that a variety of behavior is possible depending on the length of the delamination as well as the other parameters of the problem. Stable growth with eventual arrest is theoretically possible, but only in a narrow range of the normalized load. Beyond this point only unstable (or unarrested) growth is possible. In any event, it was found that the fracture energy associated with the delamination process is a dominant parameter controlling the possible growth and arrest.

The most complicated analysis consists of a two-dimensional modelling of a thin elliptic delamination in the same infinitely-thick plate. For this problem a general displacement function known to satisfy the boundary conditions is assumed for the buckled delamination. In this case the deformations take the form of an infinite series with the maximum amplitudes arbitrary at this point. These displacement expressions are then substituted into the strain energy expression for the delaminated section. According to the stationary potential energy criterion, the unknown coefficients (amplitudes) can be found from the condition that the first variation of the energy with respect to them is zero.

Essentially, this process is minimizing the stored energy with respect to the buckled displacements. This procedure, however, requires the solution of an infinite set of nonlinear equations. Assuming that the five largest terms in the strain energy expression will accurately describe the behavior, numerical techniques are used for an approximate solution.

Once the energy of the buckled delamination has been found, the same fracture criterion used for the one-dimensional model can be used to examine the energy change in the system resulting from an incremental increase in the area of a buckled delamination. This is a more complicated problem, however, since the energy release rates along the different axes of the ellipse may not be equal. When the energy release possible with a unit increase of the delamination area is maximized with respect to these two parameters, this model is able to predict the varying behavior of a buckled delamination as a function of the delamination dimensions, the load at which it is introduced and the fracture energy of the material.

When this analysis was applied to a model that simulates impact-induced delaminations, it was found that the growth of the damaged area is unstable and occurs primarily in a direction normal to the load. Impressively in agreement with experimental observations, it also predicts that higher loads will produce smaller damage extension along the load axis during delamination growth. Even more important, however, the theoretical threshold curve was found to qualitatively agree with the experimental ones. It encouragingly appears that this model might be used to describe the dominant physical aspects in the problem of delamination buckling and propagation in laminated plates.

To examine the influence of plate curvature on failure propagation mechanisms, the curved plate experiments conducted for this report were closely modelled after the experiments by Chai. Test results are presented followed by

an analytic study of the effect of plate curvature on delamination buckling.

CHAPTER 2 - IMPACT EXPERIMENTS

The problem of impact tolerance of fiber-reinforced composites has received considerable attention from private industry and governmental agencies alike. Tests on Gr/Ep laminates have been conducted to determine material responses and the behavior of semi-monocoque structures. To examine the influence of plate curvature on delaminations, experimental conditions were modelled after similar flat plate tests completed at NASA and Caltech[5]. In addition to a simplified comparison of data, similar set-ups and procedures resulted in substantial financial savings.

2.1 Experimental Apparatus and Procedures

Ballistic impact is realized by a half-inch diameter aluminum ball fired from an air gun system. A small tank is used as a reservoir for the 15 to 75 psi of air pressure used to propell the sphere. In order to synchronize the impact with the filming, a timing pulse from the camera is used to trigger a solenoid-activated valve. The pressure differential then drives the ball down one of three gun barrels used toward the test specimens. The original 15 inch gun barrel was suitable for projectile velocities of 15 to 76 meter/second, but in order to increase speeds, longer barrels with smaller projectile clearances were installed to achieve a maximum velocity of 135 meters/second. Calibration for each barrel was accomplished using the same instrumentation. With the projectile interrupting a 15 milliwatt helium-neon laser beam at two points, a photodiode coupled with a counter measured the time interval required to travel the fixed distance. Although the high-speed barrel proved to be the most reliable, all calibration tests revealed a maximum velocity scatter of about 1.5% within the range of test conditions. Errors as much as 3%, however, were found to exist for the low

5. Byers, B., ref. 3; Chai, H., ref. 4; Knauss, W. et al., ref. 6;, Rhodes, M. et al., ref. 10,11 and 12; Starnes, J. et al., ref. 13

pressure - low velocity tests. A schematic of the air gun and velocity detector is illustrated in figure 1, and velocity vs. air pressure curves are presented in figure 2.

The test specimens used in this investigation were fabricated from unidirectional Gr/Ep tape by Boeing Co. at their Everett, Washington facility. All ten panels provided were constructed using the same 48-ply layup, and individual layer and laminate properties are listed in Table 1. Ultrasonic C-scans were used to inspect for initial defects. The outer surface of the circular cylindrical panels, measured as a 15 inch radius, was used as the tool surface during fabrication. Other panel dimensions measured 12 inches by 12 inches with a thickness of .26 ± .03 inch.

In order to increase the number of experiments and better examine the influence of global parameters on the delamination mechanism, several of the panels were quartered into 6 inch by 6 inch pieces. The heterogeneous and brittle nature of Gr/Ep requires special attention during machining, however, high-speed abrasive wheels were used successfully

The two specimen support fixtures required were both constructed to duplicate the loading and boundary conditions used in similar studies. The curved edges of the test panels which were used to apply loads were ground flat and bonded to heavy aluminum bars with Devcon epoxy to approximate clamped edge conditions. Radiused edges were used for the vertical sides. While allowing motion within the plane of the undeformed middle surface, edge support attachment to very rigid stiffeners prevented any normal displacement along the line of contact. Screw adjustments provided in the stiffeners allowed correction for plate normalcy to the fixture's loading surface. Photographs of both fixtures can be found in figures 3 and 4.

Loads of up to 150,000 pounds were furnished by a Baldwin hydraulic testing machine with a ball used to assure central application of the load and relieve any moments that might be produced by wobble of the machine head. Although calibration tests revealed excellent agreement between Baldwin gages and the applied load, load distribution and intesity was also monitored with strain gages. Using 6 to 8 gages on each specimen, any bending was determined by mounting gages on opposite faces of the panels. In all cases bending was limited to a maximum of 15% of the compressive strain. St. Venant's principle held true as gages near the impact point were within 5% of the average panel values. Prior to impact, all panels were prestrained in axial compression in the range of 2800 to 5000 μ in/in. Gage locations and sample data are illustrated in figure 5.

Any impact damage or subsequent propagation was photographically recorded with a high-speed camera (Red Lake Lab Model Hycam K20S4BE). Although the camera has a maximum speed of 10,000 frames/sec, a one-quarter frame prism assembly was used to obtain photographic data at speeds up to 40,000 frames/sec. Framing rates are determined by a 1 kHz timing pulse displayed on the developed film (Kodak 2484 pan film - 16 mm b/w negative) and was generally between 32,000 and 38,000 frames/sec. All panels were impacted at the center of the convex side and photographed on the opposite side.

A Xenon flashtube supplied the high intensity light needed for such photography. A 6kV, 500 μ f capacitor bank proved to be a suitable power source, and modifications of the bank's internal wiring allowed control of the pulse intensity and duration. Using a piece of ground glass to obscure details of the light source, a convergent lens and pinhole approximated a point source. Another 8 inch lens achieved the collimation necessary for the shadow moiré technique.

Catastrophic failure by delamination is characterized by a sudden drop in the compressive load accompanied by large amplitude buckles. Moiré techniques

coupled with high-speed photography lend themselves well to examination of this mechanism on its microsecond timescale. The moiré effect is a coarse pattern of light and dark bands, subsequently referred to as fringes, produced whenever two arrays are superimposed and viewed with either transmitted or reflected light. Grids or gratings consisting of parallel, opaque lines with transparent interspaces of equal width were used during experimentation to produce this effect.

A big advantage of the moiré technique is that it provides continuous data over a large field without interfering with the test specimen. Measurements are direct and simple yet require uncomplicated illumination and observation systems. Changes of the fringe patterns are gross magnifications of the deformations which produce them, however, the inherent low sensitivity of the method is particularly attractive for problems involving large displacements. Also, various moiré methods can emphasize certain components of displacement while minimizing the effect of others. In our problem, out-of-plane displacements predomiate, and the oblique-shadow (OBS) moiré technique used determines such normal deformations while leaving the influence of in-plane displacements insignificant.

In the OBS method a grating is illuminated by a beam of collimated light to cast its shadow on the surface of the test specimen. When the shadow grid is viewed through the master grating, geometric interference produces a fringe pattern which reflects the variation of the gap between the specimen and the grating. Since diffuse refelction is employed here, a matte surface finish is required on the specimen. The best results were obtained by a light sanding of the specimen surface followed by painting with Tens-Lac U-10 undercoating. To minimize the effect of unrelated reflections, surfaces not viewed by the camera were painted flat black.

As illustrated in figure 6, when the distance between the specimen and the grid is h_1 the illuminated bands of the shadow can be seen by the observer. Accounting for the resolution capability of the eye, the pattern is viewed as a bright fringe. At a distance of h_2, only the shadows can be viewed through the transparent portions of the master. This geometric interference based on the rectilinear propagation of light is perceived as a dark band or fringe. As the specimen deforms and the gap varies, the fringe pattern seen represents normal deflection contours mapped onto the plane of the master grating.

Fringe order is determined by the number of grating lines between the entering and exiting ray, and from geometry it can be shown that the out-of-plane displacement between any two successive fringes is

$$f = \frac{P}{\tan i} \tag{2.1}$$

where P is the grating pitch and i is the angle of incidence. If the specimen is also viewed at some angle α, this equation becomes

$$f = \frac{P}{(\tan i + \tan \alpha)} \tag{2.2}$$

From this one notes that the sensitivity of the OBS method depends only on the grid pitch and the illumination and observation angles. As a result, only minimal equipment alterations were required to vary the fringe constant f between the values of 0.0164 inch and 0.0220 inch used during experimentation.

To find the actual out-of-plane displacements, the initial fringe pattern must be subtracted from the final one. This calculation was rendered insignificant by using an appropriately curved grid to simplify the initial pattern. Unfortunately, projection of a 3-dimensional image onto the 2-dimensional plane of the film does induce certain errors. Perpendicular alignment of the grid lines with respect to the axial direction of the specimen minimized this effect to the point

where it could be easily calculated. The influence of plate curvature on the angles involved was found to vary the value of the fringe constant f a maximum of 5% across the width of the plate. Also, damage width normal to the direction of the applied load was measured along a horizontal reference axis through the impact point. Plate curvature and the photographic angle of observation, however, project this axis as an elliptic arc. When calculated, this distortion was found to be insignificant for the delaminated regions of the test panels.

After considering several methods, it was determined that the best way to construct the curved grid would be to bend a flat grid to the desired shape. High quality grids are available on flat glass plates, and a 200 lines per inch (lpi) Ronchi ruling[6] was used for the grid artwork. Kodak manufactures optically clear, acrylic plates[7] treated with a high resolution photographic emulsion, and by varying the magnification the Ronchi image was photographed[8] onto the plastic plates to create grids of 60, 80, 100, and 200 lpi. Manufacturing quality is critical since line density ultimately determines sensitivity and line width to space ratios influence the width and intensity of the moiré fringes. Through microscopic inspection, it was discovered that strict control of developing times would keep these errors to less than 3%.

Visibility and the desire to avoid interference with the test specimens limited the methods by which the grid could be shaped. Adopting a brute force approach, a rigid frame was built to support the grids at the proper curvature. Taking the grid-specimen gap and moiré grid thickness into consideration, one of the Gr/Ep plates was used to construct a mold. Devcon Plastic Steel B[9] was

6. 200 lpi Ronchi ruling cut on 6"x6"x.090" glass plate. Purchased from Edmund Scientific Co., produced by Max Levy Co., Phil., PA.
7. Kodak Photoplast Plates, 8"x10"x.060" by Eastman Kodak, Rochester, NY.
8. Work done by Martin Studios, Pasadena, CA.
9. Devcon Plastic Steel B, a liquid version of the epoxy used to bond the Gr/Ep plates in the loading fixtures, has an 80% steel content which permits easy machining. Both materials were purchased from Garrett Industrial Supply of Los Angeles, CA.

used for the casting which was then machined to form two stiffeners. Following this, the edges of the plastic grid were bonded to the stiffeners using Eastman 910 adhesive. To reduce the influence of anti-classic curvature, two bars (.090 inch square steel) were also attached to the vertical edges with the same glue. The photograph in figure 7 shows the curved grids after completion.

The grid assembly was then joined at its four corners to the specimen stiffeners by the screw-spring mechanism schematically illustrated in figures 8 and 9. This device permitted adjustment of the grid location so that simple initial moiré patterns could be achieved. Adequate moiré resolution and contrast demand a small specimen-grating gap which often results in grid destruction during large out-of-plane deformation. It was hoped that the springs would absorb some of the impact energy and thereby save the master from breakage. This concept met with partial success for specimen strains below 4300 μ in/in.

Figure 10 is a photograph of the laboratory area. Except for the air gun calibration system, the above-mentioned equipment is pictured in the experimental test set up.

2.2 Results

Thick Gr/Ep panels designed to carry high compressive loads have been found to suffer a serious strength degradation as the result of low-velocity ballistic impact[10]. Catastrophic failure happens when the local impact damage spreads across the panel's width under the action of applied loads. While dynamic wave effects from the impact are believed responsible for the initial damage, propagation through the delamination buckling mechanism is often described as a "matrix associated" failure involving intraply matrix fracture possibly along with failures of the fiber/matrix bonds. Since these two phases have been experimentally associated with different timescales, the global failure

10. Knauss, W. et al., ref. 6; Starnes, J. et al., ref. 13; Williams, J. et al., ref. 16

process is described as a sequence of separate failure mechanisms. Consequently, the presentation of experimental results begins with a brief characterization of the internal damage due to impact. The threshold curve separating the results of specimens which failed catastrophically from those which continued to carry load after impact is presented next and compared with the failure curves found in similar experiments. Finally, the results from the high-speed photography are included and discussed. Conclusions are made in light of the findings of other studies.

2.2.1 Interior Damage Characterization

As mentioned earlier, concern over the effects of low-velocity impact in Gr/Ep laminates has spurred numerous experimental studies which have simulated typical hazards. In all cases it was concluded that significant internal damage results with little or no visible surface damage. Not surprisingly, observations of the curved panels consistently agree with these well established findings.

For plates which survive the projectile encounter, the only evidence of impact in the surface contact region is a small, circular depression approximately 2 mm in diameter. The opposite face, however, generally displays a small amount of spallation and fiber fracture for velocities exceeding 75 m/sec. Unfortunately, post-mortem examinations of internal damage are not as favorable. Sectioning along the impact point reveals a fracture pattern consisting of extensive intraply cracking and delaminations. Because the area near the unimpacted surface usually contains more severe damage, the region of sustained internal damage is sometimes geometrically described as a "V-shaped" region. Since this is similar to the pattern found in homogeneous, brittle plates that have been impulsively loaded on one surface, it has been postulated[11] that internal stress waves generated by the impact are responsible for the formation of the intraply

11. ASTM, ref. 1; Byers, B., ref. 3; Rhodes, M. et al., ref. 10 and 12; Williams, J. et al., ref. 16

cracks. On the other hand, delaminations which are generally concentrated near the surface opposite the impact and between layers of differing orientation are believed to be the consequence of internal stress waves interacting with interlaminar shears (ILSs). This coupling of stress waves with ILSs is further suggested by the fact that impact under load increases the initial delamination surface area. Indeed, delaminations along planes of high ILS (i.e. between layers of differing orientation) have been observed as edge failures in tensile specimens[12].

Figure 11 provides typical photographs[13] of the ballistically induced damage found in Gr/Ep plates sectioned through the impact point. While the size of the fracture area shows only a small increase with projectile velocity, larger and more numerous fracture surfaces are associated with higher kinetic energies. Applied loads during impact have the same effect in that they increase the severity of the damage without altering its basic character (i.e. intraply cracking and delamination). In any event this permanent damage is associated with matrix fracture. Controlling factors on a finer scale, however, are obscure, and the possibility remains that damage initiation and propagation also involves the integrity and failure of the fiber/matrix interface. An experimental program[14] which evaluated the influence of resin systems on Gr/Ep laminates has shown that impact damage tolerance (and subsequent propagation) can be correlated with matrix material properties. Those resin systems which demonstrated higher fracture energies also exhibited the largest damage tolerance. Consequently, the double-cantilever beam test results which were used to measure the resistance to interlaminar fracture can also be used to qualitatively assess the impact resistance of Gr/Ep composites. Because no attempt was made to correlate interlaminar fracture energy with matrix fracture energy or with the

12. Whitcomb, J., ref. 15
13. Chai, H., ref. 4
14. Byers, B., ref. 3

strength of the fiber/matrix bond, the failure mechanisms which may participate in creating damage on the microscopic level remain uncertain.

Ultrasonic inspection is commonly used as a nondestructive method for detecting internal flaws in Gr/Ep laminates. Because this technique involves a 2-dimensional imagery of a 3-dimensional situation, it provides an inaccurate measure of the type and severity of internal damage. Comparisons with post-mortem plate sectioning, however, reveal that C-scans do indicate the projected size and shape of the area of sustained damage.

2.2.2 Threshold Curve

In general when thick Gr/Ep panels are subject to low-velocity ballistic impact while under compressive load they will either fail catastrophically or incur local damage while maintaining the applied load. The threshold curve is a damage tolerance curve for the test conditions of applied strain plotted against the impact velocity. Points above the curve represent catastrophic failures while those below it are for panels which survived the impact. The graph in figure 12 provides these data for the curved plate experiments conducted for this report. The circles are used for the small plates while the squares indicate the large panel experiments. In both instances the solid symbols represent catastrophic failures and the open ones are for those specimens which did not fail upon impact. The half-filled symbols identify those specimens which demonstrated delamination buckling and/or arrested propagation without global plate failure. A summary of test conditions is listed in Table 3. Also included in the figure are the threshold curves for flat panels with the same 48-ply laminate as found by two different experimenters[15].

Although all the panels were fabricated from the same material, test specimen X-5 was not processed with the other plates. While this is not expected to

15. Chai, H., ref. 4; Rhodes, M., ref. 9

have a significant effect on test results, possible variations in material properties due to batch processing might produce scatter about the empirical threshold curve. Also worth noting, panel X-4 withstood an impact of 72 m/sec while sustaining an applied load of 4000 μin/in. Because of the small number of panels available for testing, it was decided to retest the panel to see if prior internal impact damage would have any effect on plate failure mechanisms. Surprisingly, the panel also survived (test X-4.5) the impact (at the same impact point) of 70 m/sec while maintaining the increased load of 4500 μin/in with no additional surface damage. Concluding that this panel would have similarly survived the higher strain impact had it not been previously damaged, this test result is also included in figure 12. Considering this information along with the small number of data points, experimental results were not used to form a threshold curve. However if one were to try to construct such a curve from the curved plate experiments, it appears that the large panels might warrant a separate, higher damage tolerance curve when compared with the small panel findings.

The first thing one notices is that while the curved panel data lacks exact quantitative agreement with the flat panel curves, qualitatively all results demonstrate the same behavior. The initiation of failure in the vicinity of the threshold curve is characterized by delamination buckling followed by its propagation. Because large amounts of strain energy are released during structural collapse, failures far above the curve can involve several failure modes. In an attempt to gain a greater understanding of the delamination mechanism, most tests are conducted near the conjectured failure curve. More specifically, the majority of tests are carried out over a narrow range of impact velocity (60-80 m/sec) and strain (3000-3500 μin/in) where the strength degradation due to impact is most pronounced.

The two curves presented were all constructed with limited data, and as a result they are not extremely well defined. This is not important, however, since the threshold curve is an idealization. Delaminations have been linked to matrix-associated failures and have been found to be very sensitive to the material properties of the epoxies used. During laminate construction, the prepreg is cured at high temperature (about 350° F) while the excess epoxy resin is soaked off under pressure. This is a lengthy and difficult process for thick laminates which virtually guarantees variations in material properties from the nominal values. To account for these differences, a band representing and upper and lower bound is a better representation than a solid curve.

The important thing to note is that in considering such a tolerance, plate curvature has no apparent effect on the threshold curve. Also, in these tests plate length and width have little influence on the failure threshold strain. Instead, the extent of internal damage is a key factor affecting the failure strain. Nevertheless, the mere existence of damage is enough to cause a serious strength degradation. These facts indicate that failure in the vicinity of the threshold curve is a local phenomenon independent of global parameters.

2.2.3 Photographic Results

The six photographs comprising figures 13 through 18 are the high-speed photographs of the six curved panels which catastrophically failed upon impact. With the moiré fringes representing contours of equal "out-of-plane" displacement, the fringe constant, f, is defined as the normal displacement between any two consecutive fringes. The closed-loop fringe contours evident in all the photographs vividly illustrate the shape of the buckled delaminations and their propagation. In all cases the failure begins with the circular impact damage buckling on a timescale that is less than the camera's time interval Δt. Then within the resolution of the camera's timescale, the damage spreads across the panel at a

constant velocity. Eventually the point is reached when the failure mode changes to a narrow, irregular pattern that is characterized by extensive fiber fracture. In the tabulated results, the maximum delamination width at this point of transition is referred to as w_d max.. Corresponding delamination height and maximum out-of-plane displacement are referred to as h_d max. and δ_d max. respectively. These measurements are dimensioned along with other geometric panel parameters in the schematic drawing in figure 19. The small panel specimens have been given an SX-n designation and the large ones an X-n designation. With the edge supports unable to arrest propagation, damage travels across the entire width of the plate and results in a global plate failure with virtually no residual strength. Typical photographs of the damage viewed along the plate's edge are provided in figure 20. The 45 degree disfigurations at the impact points in experiments SX-1, X-1, X-3 and X-5 depict surface spallation.

When comparing the experimental results of the small panels with those of the large panels, one notices that there is no substantial difference in the damage pattern or the propagation behavior. This finding is further evidenced in photographs taken subsequent to global plate failure. Provided in figures 21 and 22, a large and small panel are photographed together to facilitate comparison. Observations of the front and back surfaces reveal that the appearance of the final damage configuration is not significantly altered by global panel dimensions. Since applied loads were always kept well below the critical buckling load of the panels, it seems apparent that within this regime the delamination propagation mechanism is a local phenomenon independent of global parameters.

Generally speaking, the photographic sequence for catastrophic specimen failure begins with a buckled delamination that spreads in a direction that is normal to the direction of the applied load. While the initial impact-induced damage appears circular in shape, the propagating delamination shape will

sometimes assume a nearly elliptical boundary (i.e. SX-3). In other instances, the shape of the traveling delamination more closely resembles a rectangle (i.e. X-1). No correlation can be found with applied load, propagation speed, or behavior in the advanced stages of failure, so it seems that these variations in the shape of the delamination have little effect on this failure mechanism.

Another interesting feature concerning the shape of the delamination boundary involves the maximum delamination width compared to the load. For larger strains this width is noticeably smaller. Summarized in Table 2, plots of delamination width (w_d max.) vs. applied strain (ε_o) in figure 25 graphically demonstrate this finding. Also contained in the same figure and table, maximum delamination height (h_d max.) is compared to the applied load. Although not as pronounced, damage extension in the direction of the load also appears to be inversely related to the magnitude of the compressive strain. As it turns out, these tendencies can also be inferred from the final damage configuration. Located in figures 23 and 24, photographs of panels X-1 and X-5 are presented for these comparisons. In agreement with the moiré sequences, the higher strain panel (X-5) clearly demonstrates smaller damage extension along the load axis. Also as anticipated the "low-strain" failure is characterized by larger delamination spread normal to the direction of the applied load. Simplified analytic models[16] of delamination failure qualitatively predict this behavior. Perhaps also worth noting, these variations in the shape of the propagating delamination can not be determined from the damage on the impact face of the panel.

These above mentioned findings have also been observed in flat plate experiments. One might conjecture, therefore, that for this case plate curvature has a negligible influence on the conditions necessary for damage growth and its subsequent behavior. Evidence of this is provided through comparison with the

16. Chai, H., ref. 4

high-speed, flat panel photographic sequence[17] in figure 26.

Calculated values of the delamination propagation speed range between 640 and 1050 feet per second for the curved plates. Although this horizontal growth rate is seen to vary with the magnitude of the applied load, insufficient data preclude the formulation of any empirical relation. Once again citing Chai's work, this behavior appears to be substantiated by the flat plate study. For the same impact velocity, panels with larger strains consistently demonstrated faster damage spread. After a panel incurs damage exceeding its tolerance level, the strain energy of the plate must be converted to another form of energy. It is postulated that exorbitant strain energies contribute to the dynamics of the damage growth process. If this is true, higher propagation speeds should be expected for test conditions above the threshold curve. It seems safe to assume that more curved plate experiments will continue to duplicate the findings of flat plate studies.

The only unexpected behavior occurs during the advanced stages of failure for specimen X-3 (figure 17). In the last few frames the moiré fringe pattern in the region of maximum out-of-plane displacement seems to indicate that the delamination has formed two half-wavelengths in the horizontal direction. Calculations reveal that the delamination has bulged to the point of contact with the moiré grid, and this is further evidenced by the change in the background moiré pattern after frame 13. Considering the extensive surface damage due to the high impact velocity (132 m/sec), it seems that the grid's restraint of normal deformations may have contributed to the unusual damage pattern.

Three interesting cases occurred in specimens which did not fail catastrophically. The photographic sequences for these tests (SX-2, SX-5, and X-6) comprise figures 27 through 29. In the first one, SX-2, a moiré pattern resembling a

17. Chai, H., ref. 4

buckled delamination appears but fails to propagate. The nearly circular shape of 0.7 inch diameter, its location, and the time of its appearance obviously identify this damage with the impact, but the calculated deflection of 0.050 inch is uncharacteristically large for local out-of-plane deformations initiated by the impact. Even more curious, the pictures from specimens SX-5 and X-6 show buckled delaminations which begin to propagate but stop after only a short distance. Analysis for SX-5 indicates a delamination width of 1.5 inch with a maximum deflection of 0.088 inch, and the corresponding values for X-6 are 1.4 inch and 0.060 inch respectively. In all three cases, removal of the load resulted in a relaxation of the deformation with a maximum permanent deformation less than 0.015 inch. These observations, therefore, leave little doubt that the photographic sequences illustrate deflections of buckled delaminations as opposed to local impact-induced deformations. Since no other surface damage was visible, the three experiments appear to demonstrate that delamination buckling preceds failure through the remainder of the plate thickness during spread of the impact-induced damage. Also unique to these tests, the changing background moiré pattern corresponds to global plate vibrations.

While similar observations for plates impacted under load have not been found, this type of arrested damage growth has been found for plates impacted prior to loading. In Byer's study,[18] damaged panels were loaded incrementally and photographed to monitor damage propagation. Within a narrow range, a "rapid" delamination growth was followed by arrest at a new delamination size. Based on comparisons with this NASA study,[19] it appears that the test conditions for these three curved plate experiments constitute borderline cases for catastrophic failure.

---

18. Byers, B., ref. 3.

19. Byers, B., ref. 3.

In light of comparisons with other experimental studies one may conclude that the curved plate results obtained here consistently agree with the models proposed for low-velocity impact damage and its propagation under compressive load in Gr/Ep panels. The only new finding basic to this report is that when the dimensions of the damage are small compared to the panel's radius, plate curvature has a negligible effect on the conditions necessary for damage growth and the subsequent failure response of the Gr/Ep laminate.

Based on experimental evidence, delamination growth is dependent on the development of local out-of-plane buckling deformations. Because buckling produces interlaminar forces which can cause the damage to spread, it is implied that propagation mechanisms are dependent on the applied load. Post-mortem examinations of interior damage, however, point to the fact that the nature of impact damage is not appreciably altered if it is incurred while the material is under a compressive load. Considering these things along with the observed timescales, it appears that initial impact damage and delamination propagation act as separate failure mechanisms. Damage geometry and applied loads, however, do influence the specimen response to the separate failure mechanisms which govern catastrophic failure. This is further examplified by the three cases of arrested delamination growth found here. While the remaining cases duplicate the findings of flat plates impacted under load, these three observations are similar to those for damaged panels which are taken to loads just slightly in excess of those necessary for delamination buckling.

In summary, one may characterize the failure sequence as starting with impact damage followed by delamination buckling and propagation in the outer layers which eventually leads to a global plate failure involving other mechanisms. The mechanisms involving impact damage initiation and delamination propagation are both associated with failures of the matrix and matrix/fiber

bond as opposed to fiber failure. The material properties of the matrix are a unique factor in that they appear to strongly influence the conditions necessary for impact damage initiation, growth, and arrest.

CHAPTER 3 - ANALYSIS

Collection of experimental data becomes a monumental task when developing design criteria for the engineer. Instead, mathematical models must be constructed to predict structural behavior and the failure of composite materials. The large number of parameters involved and the scatter of experimental results suggest the extreme complexity in describing such behavior. It is hoped, however, that simple representations of dominant phenomena will adequately describe the ultimate response of a solid or structure.

In an earlier thesis[20] linear fracture mechanics criteria were used to determine the conditions for growth and stability of buckled delaminations in flat panels. It was decided that before attempting this analysis for the more complicated problem of delaminations in a curved plate, the buckling behavior of flat and curved panels should be analytically compared.

3.1 Theoretical Background

Stability is based on the dynamic response of a system. An equilibrium state of a structure is considered stable if and only if motions resulting from a sufficiently small disturbance remain in the vicinity of that equilibrium state. For static conservative systems the minimum potential energy criterion can be used to determine stability.

The assumptions of the linear theory of elasticity imply that the deformations of a structure do not affect the action of the applied loads. In practice this means that one need only consider applied loads as acting on the undeformed configuration of the body. When coupled with linear constitutive relations, the principle of supersposition can be applied during analysis. While this is a suitable approximation for many problems, it can not be employed in cases

20. Chai, H., ref. 4

concerned with structural stability. Buckling, therefore, requires a nonlinear equilibrium analysis where the nonlinearity is introduced geometrically as the interaction between forces and moments and the rotations of structural elements. Rotations are not zero in linear theory, but their interaction with loads is assumed to be negligible.

To derive the necessary nonlinear equilibrium equations, one can examine the structural element in a slightly deformed configuration. Since an exact geometric description of large deformations leads to extreme analytic difficulty for many problems, the simplifying assumptions associated with the class of "intermediate" deformations are employed. In practice this means that rotations remain small (but not negligible) and nonlinear interaction between transverse shearing forces and rotations are negligible. More specifically for the thin, circular cylindrical shell, the only quadratic terms retained in the kinematic expressions involve the rotations ($w_{,x}$ and $w_{,y}$) relative to the "in-plane" axes of the shell. As an alternative to this balance of forces approach, the principle of stationary potential energy can be used to derive the same differential equations of equilibrium. According to this theorem, a structure is in equilibrium if its potential energy is stationary. This is equivalent to having the first variation of the total potential energy equal to zero (i.e. if the integrand of the potential energy expression for the body satisfies the Euler equations of the calculus of variations). In this derivation geometric nonlinearity is introduced through the kinematic relations.

In the following analyses of circular cylindrical shells, the assumptions of thin shell theory and the quasi-shallow shell approximations are adopted.

3.1.1 Classical Theory

Solutions of the nonlinear differential equations of equilibrium will determine

the equilibrium paths of a buckled structure. Only in a few simple cases, however, it is possible to obtain closed form solutions, and numerical techniques are often necessary for approximate solutions. The purpose of "classical" stability theory is to determine the critical load (i.e. the smallest load at which the equilibrium of a structure fails to be stable) by solution of linear differential equations.

The two most common methods used to find the linear stability equations employ the adjacent-equilibrium and minimum potential energy criteria. To begin with both techniques assume an unbuckled displacement configuration, the fundamental state, which satisfies the equilibrium equations and the boundary conditions of the structure under consideration. The possible existence of neghboring equilibrium configurations is then investigated.

The adjacent-equilibrium criterion accomplishes this by using a perturbation technique to examine the two neighboring equilibrium states. Arbitrarily small increments are added to the displacements of the fundamental state, and this new deformation field is substituted into the nonlinear equations of equilibrium. Because the fundamental state is an equilibrium configuration, terms that do not contain the incremental displacements equate to zero. Furthermore, since these additional displacements are assumed infinitesimal only their first order terms need be retained in the equations. This procedure yields a set of linear differential equations (the linear stability equations of classical theory), the solution of which determines the critical load and the associated buckling mode(s).

For static, conservative systems, a structure is in stable equilibrium if its potential energy is a relative minimum. According to the Trefftz criterion, this condition for loss of stability is equivalent to having the integrand in the expression for the second variation of the potential energy satisfy the Euler

equations of the calculus of variations. To obtain the second variation of the total potential energy, arbitrarily small incremental displacements are added to the equilibrium configuration of the fundamental state. The potential energy increment between the two equilibrium configurations is examined with the second variation of the increment found by collecting all terms that are quadratic in the incremental displacements. Introduction of the integrand of the second variation expression for the potential energy increment of the body in accordance with the Trefftz criterion yields the linear stability equations.

To simplify the stability analysis of circular cylindrical shells, prebuckling rotations of the fundamental state are ignored. This leads to a set of linear differential equations with variable coefficients which are governed by the linear equations of equilibrium. Essentially this simplification permits one to examine the buckling of a cylinder under the action of in-plane loads as a bifurcation problem. This analysis leads to a linear eigenvalue problem the solution of which indicates the load and initial mode of the buckling pattern which begins to develop at the bifurcation point. Unfortunately, as a consequence of the simplifications of linear stability theory no information is obtained about the initial slope or shape of the postbuckled equilibrium path. Also, by omitting prebuckling rotations the influence of initial imperfections can not be considered.

3.1.2 Initial-Postbuckling Theory

In Koiter's analysis[21], the principle of stationary potential energy applied to the energy increment between the fundamental and a neighboring configuration at the critical load yields a set of linear differential equations, the solution of which describes the initial portion of the buckled equilibrium paths. The configuration of the neighboring state is defined as the fundamental state plus small incremental displacements in the form of the classical buckling mode. At

21. Koiter, W., ref. 8

this point the energy increment between these assumed states is expanded as an asymptotic series. Variational energy theorems applied to the increment will provide the differential equations which govern the secondary path, however, one must find these solutions from nonlinear differential equations. In his thesis, Koiter rigorously proves that the first and second-order displacement terms are the dominant expressions in the energy increment. Using this approximation for the potential energy, the differential equations of the variational problem are linear in terms of the incremental displacements yet reveal the initial slope and curvature of the secondary path. His theory is correct in an asymptotic sense in that he is exact at the bifurcation point and a good approximation for configurations in the nearby vicinity. In comparison with classical stability theory, one notices that essentially he is using a better approximation for the energy of the buckled structure.

This analysis derived from energy considerations also lends itself for investigating initially imperfect structures. In practice any deviations from the perfect realization will induce bending in the fundamental state. Koiter accounts for this by merely adding an appropriate term to the energy increment. Due to the difficulty in precisely measuring actual imperfections and to reduce the calculations required, he assumes imperfections in the shape of the classical buckling mode. Results indicate that for systems with unstable secondary paths, there is a larger reduction in the magnitude of the critical buckling load due to initial imperfections.

To summarize his main result, the type of postbuckling behavior is governed completely by the slope and curvature of the postbuckling curve at the critical load. According to the initial-postbuckling theory, if neighboring equilibrium states exist at loads below the critical buckling load they are always unstable under prescribed loading conditions. If the neighboring states exist at loads in

excess of the critical value, usually they are stable.

3.2 Theoretical Application and Results

Application of the linear stability theory has been used to determine the buckling load of a cylindrical shell under uniform axial compression. For long cylinders with simply-supported edges, classical theory predicts the existence of many buckling modes, including an axisymmetric mode, at the same critical load. The value of this load is found from

$$\lambda_{cr} = \frac{\sigma_{cr}}{E} = \frac{t}{R\sqrt{3(1-\nu^2)}} \tag{3.1}$$

This approximation, however, is unsuitable for shorter cylinders. At some point, only one half-wave will form in the axial direction, and in the limit the critical load is seen to approach Euler's formula for an elemental strip or

$$\lambda_{cr} = \frac{\sigma_{cr}}{E} = \frac{\pi^2 t^2}{12\,(1-\nu^2)l^2} \tag{3.2}$$

From the eigenvalue problem, it can be shown that for the condition

$$\left\{\frac{\pi R}{l}\right\}^2 \leq \frac{2R}{t}\sqrt{3(1-\nu^2)} \tag{3.3}$$

fluctuations of the critical load are small, and the long cylinder estimation of equation (3.1) is adequate.

In what is later used to model the behavior of an axially stiffened cylinder, Timoshenko[22] examines the problem of a curved panel in axial compression. Using the same equations and methods, he satisfies the boundary conditions for simply supported edges by making the displacement expressions periodic with respect to the panel angle β. Wide panels with similar length dimensions are expected to buckle into a large number of waves, and from this he concludes that the panel will buckle at the same stress as for the axisymmetric buckling of

22. Timoshenko, S., ref. 14

a long cylinder (equation (3.1)).

For small values of β, the panel will circumferentially buckle as one half-wave. As the radius of the shell becomes larger, the magnitude of the critical stress will approach that for a long, flat plate or

$$\lambda_{cr} = \frac{\pi^2 t^2}{3(1-\nu^2)b^2} \tag{3.4}$$

Timoshenko goes on to conclude that for the condition

$$\beta R \geq 2\pi \left(\frac{R^2 t^2}{12(1-\nu^2)} \right)^{.25} \tag{3.5}$$

the buckling load becomes equal to that found for the long cylinder. If the panel is too narrow to satisfy the above inequality the buckling load becomes

$$\lambda_{cr} = \frac{\pi^2 t^2}{3(1-\nu^2)(R\beta)^2} + \frac{\beta^2}{4\pi^2} \tag{3.6}$$

Although he is able to demonstrate the influence of shell curvature on the magnitude of the critical stress, Timoshenko is unable to elucidate the post-buckled behavior of curved panels.

After establishing boundary conditions and the buckling mode, the initial-postbuckling analysis can be extended to the behavior of curved panels[23]. In agreement with classical theory, any wide plate satisfying the inequality (3.5) will behave like a complete cylinder and buckle at the critical load indicated by equation (3.1). If the panel does not meet this criterion, the panel width enters as a periodic term in the displacement equations describing the buckling modes. Again the values for the critical load are in agreement with linear stability theory.

23. Koiter, W., ref. 7

$$\lambda_{cr} = \frac{\sigma_{cr}}{E} = \frac{\pi^2 t^2}{3(1-\nu^2)b^2}(1+\vartheta^4) \tag{3.7}$$

where curvature parameter ϑ is defined by

$$\vartheta = \frac{1}{2\pi}\left(12(1-\nu^2)\right)^{.25}\frac{b}{R}\sqrt{\frac{R}{t}} \tag{3.8}$$

Results for the simply-supported flat plate and the circular cylinder are found by taking ϑ to the limiting values of zero and one, respectively.

At the critical load the postbuckling curve in terms of compressive strain ε and the nondimensional load λ is given by

$$\varepsilon = \lambda + \frac{\lambda-\lambda_{cr}}{1-2\vartheta^4-9S} \tag{3.9}$$

where $0 \leq \vartheta \leq 1$ and S is defined by

$$S = \sum_{n=1}^{\infty}\left[\frac{1}{(n^2+1)^2} + \frac{(n^2+1)^2}{\vartheta^4} - 1 - \frac{1}{\vartheta^4}\right]^{-1} \tag{3.10}$$

$$F = 1 - 2\vartheta^4 - 9S \tag{3.11}$$

Real solutions are possible only if $\lambda \geq \lambda_{cr}$ when F is positive, and for $\lambda \leq \lambda_{cr}$ if F is negative. Since stable equilibrium configurations in the initial postbuckled regime do not exist at loads less than the buckling load, the stability of a narrow curved panel is specified by the sign of F.

This theory, therefore, describes the continuous transition from the stable behavior of the very narrow panel to the highly unstable one of an unstiffened cylinder. The change occurs in the range of a narrow panel ($0 \leq \vartheta \leq 1$) for a value of $\vartheta = 0.64$.

Initial imperfections are assumed in the shape of the classical buckling mode, and for small amplitudes, the effect on the magnitude of the critical load is found from

$$-2|\mu|\,\lambda_\mu + \frac{8}{9}\sqrt{\frac{2}{1-\nu^2}}\sqrt{\frac{1+\vartheta^4}{(-F)}}\left\{1-\lambda_\mu\right\}^{3/2} = 0 \qquad (3.12)$$

where μ , the nondimensional factor expressing imperfection amplitude, a, in terms of thickness, t, is

$$\mu = a/t \qquad (3.13)$$

and λ_μ is the normalized buckling load for an imperfect panel as defined by

$$\lambda_\mu = \frac{\lambda_{cr}(\mu = a/t)}{\lambda_{cr}(\mu = 0)} \qquad (3.14)$$

Numeric results indicate that the critical load is most sensitive to imperfections when postbuckled states are unstable and the displacement shapes considered take the form of the critical buckling mode.

The initial-posbuckling behavior of a narrow cylindrical panel can be easily understood through graphic representation of the buckling equations. Since an unbuckled delamination will not propagate, determination of the critical load is of major importance for experimental comparison.

The plot in figure 30 attempts to demonstrate the effect of plate curvature on the buckling load. The ordinate variable λ^* is the bifurcation point load normalized with respect to the corresponding load of a simply-supported flat panel sharing the same geometry and material properties. Using equation (3.4) for the flat plate load λ_{fl} and equation (3.7) for the curved plate value, λ^* is defined as

$$\lambda^* = \frac{\lambda_{cr} - \lambda_{fl}}{\lambda_{fl}} \qquad (3.15)$$

Plate curvature is determined by the parameter ϑ and plotted along the abscissa. When ϑ is zero, a value of λ^* also equal to zero appropriately indicates a buckling load equal to that of the flat plate. As plate curvature increases, the buckling load increases exponentially until the value for the complete

unstiffened cylinder is reached at $\vartheta = 1.0$. This plot, therefore, illustrates that for values of ϑ less than 0.3 plate curvature has a negligible influence on the magnitude of the critical stress. For plates with values of ϑ below this assumed limit of 0.3, a flat plate analysis seems entirely adequate to predict the conditions necessary for delamination buckling.

The bifurcation analysis is an idealization used to approximate the limit point behavior encountered in many real structures. In weight-critical design applications, however, this simplification is useful only when buckled equilibrium configurations exist at loads above the critical stress. For example, imperfections in circular cylindrical shells will convert the behavior to snap buckling at a limit point below the value of the bifurcation load. Koiter's theory uses the initial slope of the buckled equilibrium path to determine the location of neighboring equilibrium states. Since this information is found from the value of F defined in equation (3.11), the curve in figure 31 defines the initial-postbuckled stability of a curved plate. Again, curvature parameter ϑ is plotted along the abscissa to facilitate comparison with the flat panel and the complete cylinder. In the limit of $\vartheta = 0.0$ the curved plate degenerates to a flat panel, and this is indicated by the asymptote at $F = 1.0$. Similarly, in the limit $\vartheta = 1.0$ the curved plate behavior is identical to that of the cylinder - therefore the line at $F = -5.544$. With the curve beginning tangent to the flat plate asymptote, initially there is very little change in F for increasing ϑ. As a result one notices that there is very little difference between a flat panel and a curved one with a value of ϑ less than 0.3. A value of $F = 0.0$ indicates an indeterminant load-deflection relationship similar to that of a buckled column, so stable postbuckled equilibrium configurations are possible only for values of ϑ less than 0.64. Consequently, in addition to determining the range of the flat plate approximation, this curve also defines the range for the simplified bifurcation analysis.

Figure 32 represents the buckled and unbuckled stress-strain curves (equilibrium paths) for eight different curved panels identified by their value of ϑ. So they can all share the same fundamental path and bifurcation point, loads and strains are normalized with respect to their critical values. Since this plot is generated from Koiter's analysis, the postbuckled curves are the tangents in the vicinity of the buckling load. As before, $\vartheta = 0.0$ and $\vartheta = 1.0$ respectively describe the flat panel and unstiffened cylinder. Here the changing slope illustrates the transition from the stable behavior of a flat panel to the unstable behavior of a cylindrical shell within the range of a narrow panel ($0 \leq \vartheta \leq 1$). One notices that the slope decreases so slowly for ϑ less than 0.5, the curves for $\vartheta = 0.0$ and $\vartheta = 0.3$ are barely distinguishable - another justification for the flat plate approximation in this range.

Figure 33 attempts to illustrate the drop in the buckling load as a function of the amplitude of the initial imperfection waves for various values of the curvature parameter ϑ. The sharp initial slopes of these curves reveal how small imperfections can drastically reduce the magnitude of the critical load. It is also apparent how increasingly unstable postbuckled behavior contributes to this effect. Inasmuch as these curves determine the limit point load normalized with respect to the bifurcation load of the perfect panel, the analysis is inapplicable for stable postbuckled paths corresponding to ϑ less than 0.64.

At this point it becomes apparent from the initial-postbuckling theory that the adequacy of a flat plate approximation for curved panels can be determined from the value of the curvature parameter. To relate this to the experimental study, typical delamination sizes and thicknesses are used to create the carpet plot for ϑ in figure 34. Plotted along the abscissa, delamination diameter (as measured in the first frame of the moiré sequences) is substituted for panel width in equation (3.8). Listed in Table 3 as b_i, this initial delamination size was

found to vary between 0.60 and 0.92 inch. Based upon post-mortem examinations of impacted flat plates, the curved panel layup and the fact that delaminations often occur between layers of differring orientation, four curves are provided for thickness of 2, 4, 6 and 8 plies (0.011, 0.021, 0.032 and 0.042 inch. Assuming material homogeneity, values for Poisson's ratio are determined from the number of plies and the laminate stacking sequence. Ratios of 0.78, 0.66, 0.715 and 0.66 were used for the 2, 4, 6 and 8-ply curves respectively.

From figure 34 one concludes that the influence of curvature is most pronounced for the thinnest laminate (t=0.011 inch). On this curve ϑ is seen to vary between 0.35 and 0.53 within the range of experimentally observed widths (0.60 to 0.92 inch). While this is above the 0.3 limit established for the flat plate approximation, it should be noted that $\vartheta = 0.53$ results in a buckling load that is only 8% higher than that of an equivalent flat plate. Referring to figure 32, one also discovers that the initial-postbuckled curve for $\vartheta = 0.5$ remains close to the flat panel curve. With ϑ always remaining less than the stability limit of 0.64, it is implied that even in the worst experimental case the curved delamination will exhibit an insensitivity to initial imperfections similar to that of the flat plate. The geometry of the test panels, therefore, is seen to lie near the boundary of curvature insensitivity. Consequently, a flat plate approximation seems suitable for shallow, curved panels.

Based on the information from figure 34, the graph in figure 35 calculates the buckling load for the four laminates as a function of width b_i. An upper limit of 10,000 μin/in was used since other problems arise when Gr/Ep is strained in compression beyond this limit. In all four cases examined, the solid curves represent the buckling load for curved panels while the phantom-line curves plot the critical load for the equivalent flat panel. These two sets of curves clearly demonstrate that although the percentage increase in the theoretical

buckling load may be significant for "wide" delaminations, the actual increase remains small when compared with the experimentally applied loads.

As another important finding, this plot predicts that delamination buckling (and therefore any subsequent propagation) is likely only when interlaminar separations are located near the outermost layers of a laminate. Unless delamination dimensions exceed the maximum observed width of 0.92 inch, the critical loads for the 6 and 8-ply laminates are considerably higher than typical design allowables for Gr/Ep structures. Because lamina failures confined to the outer four layers of a thick laminate are not expected to appreciably reduce overall strength, one might conjecture that other failure mechanisms involving internal damage invariably must occur during global plate failure.

To collectively summarize the findings of figures 32, 34, and 35, curvature should theoretically have little effect on the critical load and initial-postbuckled stability of delaminations observed in the curved plate experiments. Since aircraft structures generally have curvatures that are much larger than the 15 inches of the test panels, a flat panel analysis should be adequate to model the delamination failure mechanism in shallow, curved panels.

3.2.1 Discussion and Conclusions

While Koiter's analysis provides an understanding of postbuckled behavior that linear stability theory makes no attempt to explain, its application to delaminations in curved plates still has limitations. In addition to establishing a range of validity for simplifying approximations, one must also be concerned with the accuracy of modeling physical systems and the possible consequences of misrepresentations.

When comparing the curved plate analysis with experimentally observed delaminations, the first thing one notices is the discrepancy in the shape of the

boundary. Photographs reveal that impact-induced delaminations are initially "circular" and propagate along the major axis of an "ellipse" normal to the direction of the applied load. Assuming a rectangular boundary with the dimensions of the elliptic axes will obviously have a nonconservative influence on the magnitude of the buckling load, but this approximation is necessary if comparisons are to be made with both the flat plate and the unstiffened cylinder. Interestingly enough, delaminations in the advanced stages of propagation sometimes resemble the assumed rectangular shape. Based on comparison of test results, these variations in shape appear to have little influence on the delamination failure mechanism. As far as the Koiter analysis is concerned, this is of no consequence. The initial-postbuckling theory can only predict the load necessary for buckling and the early stability. Beyond this point, deflections exceed the smallness assumptions and render the theory ineffective. Even if the deflections were to remain small, it is unlikely that the load distribution would resemble the uniform end shortening assumed. Without this load assumption the corresponding constant coefficients of the stability equations for the axially compressed cylindrical panel would become variable.

It is well established that if the geometry and boundary conditions of a structure match those conditions found in the appropriate section of a larger structure, analysis of the latter can be used to describe the behavior of the more specific problem. Simply-supported boundary conditions are employed for the curved plate analysis so that edge conditions can match those found in complete cylindrical shells. This requirement, however, is not a general restriction of the initial-postbuckling analysis. Instead one should note that calculation of the energy increment in specific applications demands a knowledge of the deformations in a slightly buckled configuration. By imposing simply-supported conditions along all four boundaries, buckling deflections can be specified in a form

that is periodic in both the axial and circumferential directions. As a result, the displacement functions predicted by classical stability theory for the cylindrical shell can be adapted for use in the curved panel analysis.

Unfortunately, the edge of a delamination is best represented by a clamped boundary condition. It is worth nothing, however, that rotational edge constraints along the curved edges of a cylindrical panel have been found[24] to have little influence on the magnitude of the buckling load when the length is significant ($\ell > 2b$). This same result has also been found for the longitudinal edges if the panel is wide with respect to its length. Rotational constraints along the edges of a square panel, however, will result in an appreciable modification of the buckling mode and an increase in the critical stress. With clamped edges, therefore, curved panels can be expected to be stable at higher values of ϑ.

In another item of concern, the energy increment in the initial-postbuckling analysis is based on a linear elastic material response. The macroscopic behavior of Gr/Ep laminates obeys Hooke's law, but problems do arise when the material is stressed near its ultimate strength. This becomes irrelevant here because buckling problems of interest usually do not involve elastic failure in the initial-postbuckled regime. A more important concern is the modeling of Gr/Ep as a homogeneous, isotropic solid. This material description, however, has been found to be sufficiently accurate for structural models used to understand physical phenomena.

When discussing the discrepancies between the physical problem and the theoretical model, one should note the intent of the initial-postbuckling analysis used in this report. As mentioned earlier, the previously solved problem of a thin, elliptic delamination in a flat plate has been used with relative success to describe the delamination propagation mechanism experimentally observed in

24. Timoshenko, S., ref. 14, Hutchinson, J. et al., ref. 5

flat, Gr/Ep laminates. The purpose of the Koiter analysis is merely to justify Chai's work as a suitable flat plate approximation for curved panels. According to the results of the previous section, a curved panel with a curvature parameter ϑ equal to 0.3 will have a critical buckling load less than 1% higher than that of the comparable flat panel. Perhaps more important, the theoretical initial-postbuckling curves for the two panels are virtually indistinguishable. Since values of ϑ for impact-induced delaminations in Gr/Ep plates are typically on the order of this 0.3 "limit", the flat plate approximation seems entirely appropriate. Observations from the curved plate experiments substantiate this conclusion.

Due to the unavoidable presence of imperfections, the buckling of flat plates is often so gradual that it is impossible experimentally to precisely determine the load at which buckling is said to occur. This can be attributed to the fact that plates with supported edges can accept additional load after buckling. Best examplified by the flat plate, "effective width" design analyses are based on this stabilizing influence of the edge supports which prevent buckling over the entire width of the plate[25]. Similar to the flat plate, the supported edges of a curved plate are expected to be able to withstand additional load following buckling. Based on this information, one might intuitively expect the behavior of a narrow curved panel ($0 \leq \vartheta \leq 1$) in the advanced postbuckling stage to approach the behavior of a flat panel of equal width. Figure 36, therefore, offers the conjectured postbuckling curves for narrow cylindrical panels. If this speculation could be confirmed either by analysis or experiment, it has been postulated[26] that a detailed knowledge of the complete postbuckling curve for narrow panels would be of little practical interest since the part of the curve substantially above the curve for a flat panel is highly sensitive to initial imperfections.

25. Timoshenko, S., ref. 14, Brush, D. et al., ref. 2
26. Koiter, W., ref. 7

CHAPTER 4 - SUMMARY

Thick, Gr/Ep laminates are known to suffer a serious strength degradation due to low-velocity ballistic impact. When plates are impacted while under compressive load, locally incurred damage may propagate to the undamaged regions of the plate through delamination buckling and delamination growth. In an attempt to gain a greater understanding of this process which can lead to catastrophic plate failure, typical runway hazards were simulated in an experimental study. Test conditions and procedures were modelled after earlier investigations, and plate curvature was introduced to examine the influence of this global parameter on the delamination failure mechanism.

Two sizes of circular cylindrical panels were used for this study, however, all specimens were constructed using the same 48-ply layup and 15 inch radius of curvature. The large plates measured 12 inches along each side while the small plates (cut from the large plates) have 6 inch sides. In all cases supported and clamped boundary conditions were provided for the axial and circumferential edges respectively while the panels were loaded in axial compression (2800 μ in/in to 5000 μ in/in) prior to impact. An air gun system was used to propel a 1/2-inch diameter aluminum ball normal to the plate's outer surface at speeds ranging between 59 m/sec and 132 m/sec. High-speed photography coupled with an oblique-shadow moiré technique was employed to record initial delamination buckling and subsequent propagation on the surface opposite the impact face.

Initial impact damage consists of intraply cracking and layer separation with larger and more numerous fracture surfaces generally located near the surface opposite the impact face. Similar to the pattern found in brittle plates, impact-induced stress waves are believed to be responsible for this internal damage.

The delamination mechanism which can lead to global plate failure, however, has been experimentally identified as a separate failure process which occurs on a much longer timescale (μ sec for initial damage vs. msec for delamination propagation).

In most tests of this type, plates either incur a local area of damage while sustaining a large percentage (about 95%) of the applied load or have the damage spread across the entire width of the plate as most of the plate's stored strain energy (about 95%) is released. The threshold curve is the damage tolerance curve separating catastrophic failures from surviving panels found when applied strain is plotted against impact velocity. Results indicate that when applied loads remain well below the global buckling load, panel size has a small influence on the location and shape of this curve. To investigate the effects of plate curvature, comparisons are made with the experimental threshold curves found from flat panels made with the same material and layup. Findings indicate that in the vicinity of the threshold curve, curvature has no substantial effect when the initial damage width is small compared to the plate's radius of curvature.

Photographic sequences clearly demonstrate that the catastrophic failure process begins with local buckling of the impact-induced delamination. The buckled delamination is then observed to spread in a direction normal to that of the applied load through fracture of the epoxy matrix and/or along the fiber/matrix interface. Once again, comparison with similar flat panel data apparently shows that in this instance plate curvature is not a significant factor influencing the nature and spread of the damage.

To obtain a better understanding of the factors controlling damage growth, a recent analytic study by Chai attempts to model the delamination growth mechanism. Based on large deflection plate theory and fracture criteria, a

simplified representation of a thin delamination in a flat plate reveals that initial delamination size, applied load, and fracture energy are the dominant parameters controlling damage growth and possible arrest. This analysis is able to adequately predict the type of behavior found in experimental studies, and his theoretical threshold curve is qualitatively in agreement with the experimental ones. The prediction that fracture energy is the predominant factor controlling damage arrest is also substantiated by various studies assessing the influence of different resin systems on damage tolerance. It therefore encouragingly appears that this simplified analysis can be helpful when seeking to improve the impact resistance of laminated materials. With this in mind, an analytic investigation was conducted for this report to determine the influence of plate curvature on delamination buckling. If a cylindrical panel is very narrow or has a very large curvature, the behavior is expected to be similar to that of a flat panel. This was shown to be true in the initial-postbuckling analysis of a narrow, curved panel. Since the curvatures of aircraft structures are usually much larger than the 15 inch radius of the test specimens, the previously solved flat plate problem should be adequate to predict the conditions necessary for delamination buckling and propagation in Gr/Ep laminates.

In summary, the initial-postbuckling theory justifies a flat plate analysis if the delamination width is small compared to the plate's radius. Observations from the curved plate experiments are in agreement with this finding.

BIBLIOGRAPHY

1. American Society for Testing and Materials, "Foreign Object Impact Damage to Composites," American Society for Testing and Materials, 1975.

2. Brush D. and Almroth, B., "Buckling of Bars, Plates, and Shells," McGraw-Hill, 1975.

3. Byers, B., "Behavior of Damaged Graphite/Epoxy Laminates Under Compression Loading", NASA CR 159293, 1980.

4. Chai, H., "The Growth of Impact Damage in Compressively Loaded Laminates," Ph.D. Thesis, California Institute of Technology, Pasadena, California, 1982.

5. Hutchinson, J. and Koiter, W., "Postbuckling Theory," Applied Mechanics Reviews, Vol. 23, 1970.

6. Knauss, W., Babcock, C. and Chai, H., "Visualization of Impact Damage of Composite Plates by Means of the Moiré Technique," NASA CR 159261, 1980.

7. Koiter, W., "Buckling and Postbuckling Behavior of a Cylindrical Panel Under Axial Compression," NLR Report S 476, 1956.

8. Koiter, W., "On the Stability of Elastic Equilibrium," NASA TT F-10, 1967.

9. Rhodes, M., "Damage Tolerance Research on Composite Compression Panles," NASA CP 2079, 1980.

10. Rhodes, M., Williams, J. and Starnes, J., "Effect of Impact Damage on Compression Strength of Filamentary-Composite Hat-Stiffened Panels," SAMPE, Vol. 23, 1978.

11. Rhodes, M., Williams, J., and Starnes, J., "Effect of Low-Velocity Impact Damage on the Compressive Strength of Graphite-Epoxy Hat-Stiffened Panels," NASA TN D-8411, 1977.

12. Rhodes, M., Williams, J. and Starnes, J., "Low-Velocity Impact Damage in Graphite-Fiber Reinforced Epoxy Laminates," Society of the Plastics Industry, Presented at 34th Annual Conference, New Orleans, La., 1979.

13. Starnes, J., Rhodes, M. and Williams, J., "The Effect of Impact Damage and Circular Holes on the Compressive Strength of a Graphite-Epoxy Laminate," NASA TM 78796, 1978.

14. Timoshenko, S. and Gere, J., "Theory of Elastic Stability," McGraw-Hill Book Co., 1936.

15. Whitcomb, J., "Experimental and Analytic Study of Fatigue Damage in Notched Graphite-Epoxy Laminates," NASA TM 80121, 1979.

16. Williams, J., Anderson, M., Rhodes, M., Starnes, J. and Stroud, W., "Recent Developments in the Design, Testing and Impact Damage Tolerance of Stiffened Composite Panels," NASA TM 80077, 1979.

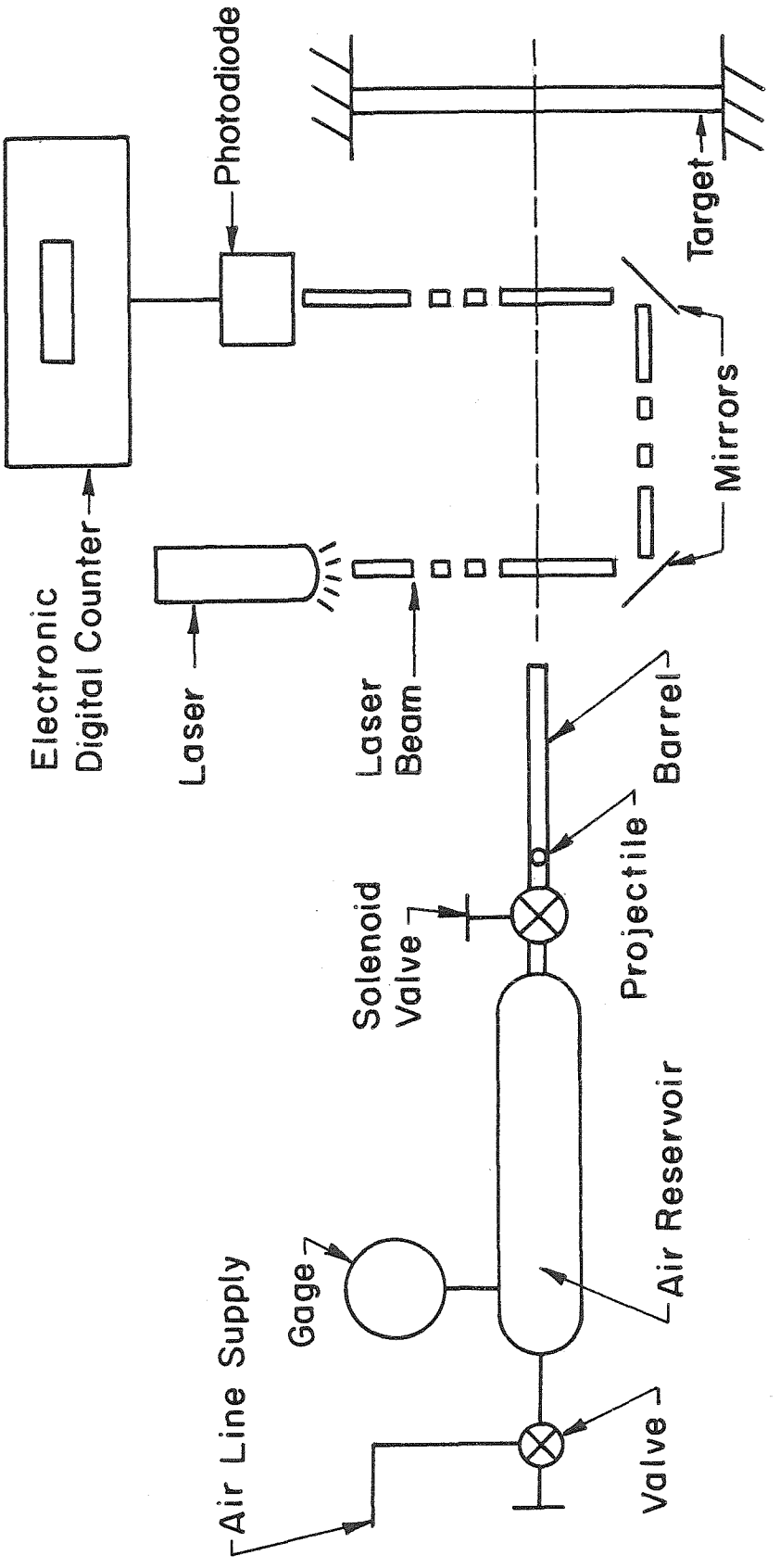

FIG. 1 SCHEMATIC DRAWING OF AIR GUN AND VELOCITY DETECTOR

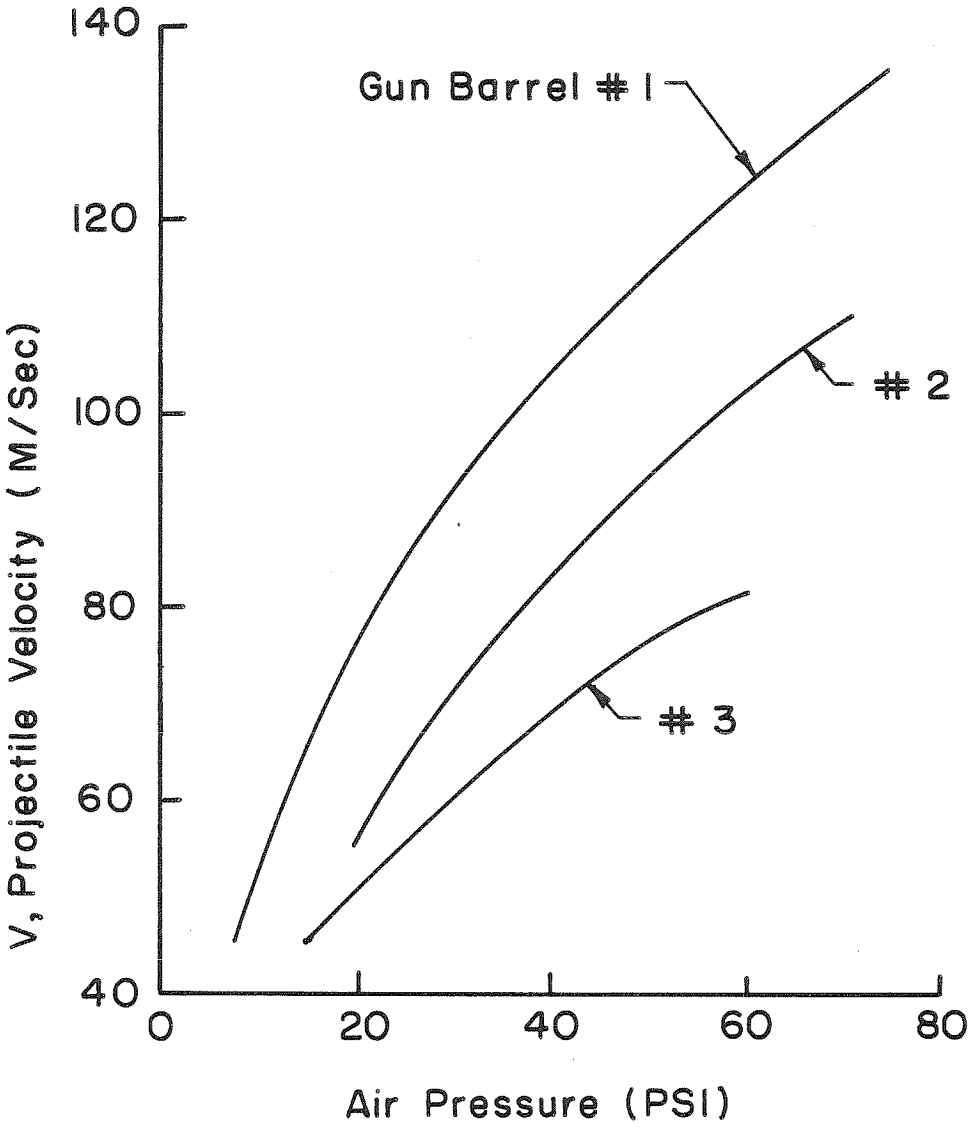

FIG. 2 VELOCITY VS. AIR PRESSURE

Table I - Material Properties for T300/5208 Graphite/Epoxy

Lay Up: $(+45/-45/0/0/+45/-45/0/0/+45/-45/0/90)_{2S}$

Nominal Ply Properties

Longitudinal modulus, $E_1 = 19.00 \times 10^6$ psi

Transverse Modulus, $E_2 = 1.89 \times 10^6$ psi

Shear Modulus, $G_{12} = 0.93 \times 10^6$ psi

Major Poisson's ratio, $\nu_{12} = 0.38$

Ply thickness = 0.0055 in. (0.14 mm)

Density = 0.055 lbm/in^3 (1.52 g-cm^3)

Laminate Stiffness Properties

Dimension: A_{ij}: 10^6 x lbf/in. (=0.176 GN/m)

D_{ij}: 10^3 x lbf-in. (112.98×10^{-9} N-m), i,j= 1,2,6

$$\begin{bmatrix} N_x \\ N_y \\ N_{xy} \\ M_x \\ M_y \\ M_{xy} \end{bmatrix} = \left[\begin{array}{ccc|ccc} 3.03 & 0.72 & 0.00 & & & \\ & 1.51 & 0.00 & & 0 & \\ \text{SYM.} & & 0.77 & & & \\ \hline & & & 17.71 & 4.57 & 0.23 \\ & 0 & & & 7.88 & 0.23 \\ & & & \text{SYM.} & & 4.88 \end{array}\right] \times \begin{bmatrix} \partial u/\partial x \\ \partial v/\partial y \\ \partial v/\partial x + \partial u/\partial y \\ -\partial^2\omega/\partial x^2 \\ -\partial^2\omega/\partial y^2 \\ -2\partial^2\omega/\partial x \partial y \end{bmatrix}$$

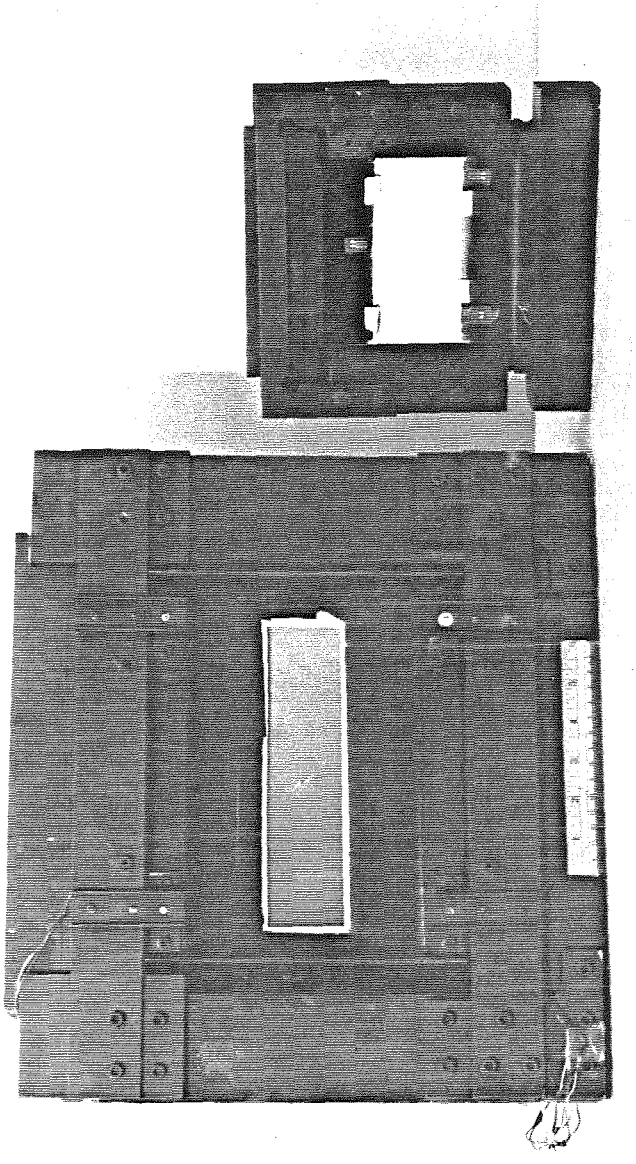

FIG. 3 LARGE AND SMALL TEST FIXTURES - MOIRÉ FACE

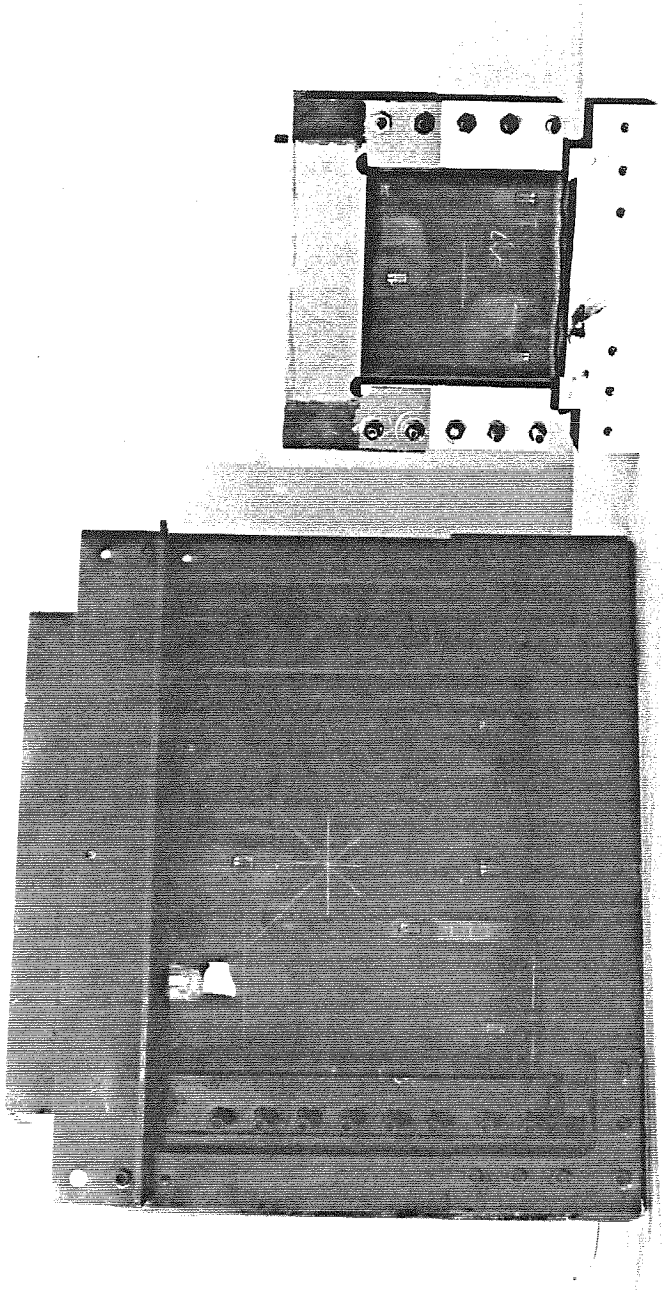

FIG. 4 LARGE AND SMALL TEST FIXTURES - IMPACT FACE

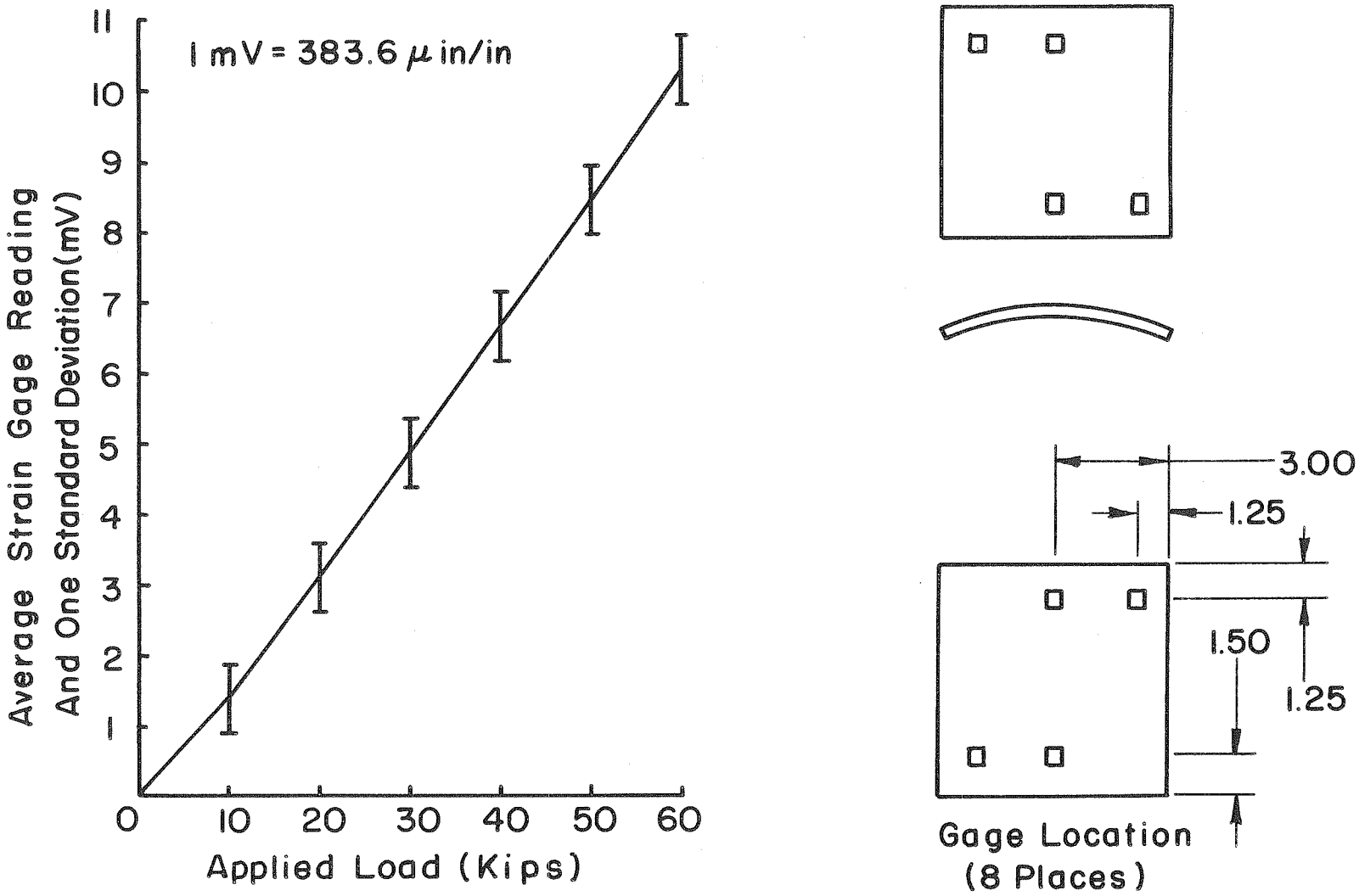

FIG. 5 SX-1 STRAIN GAGE DATA

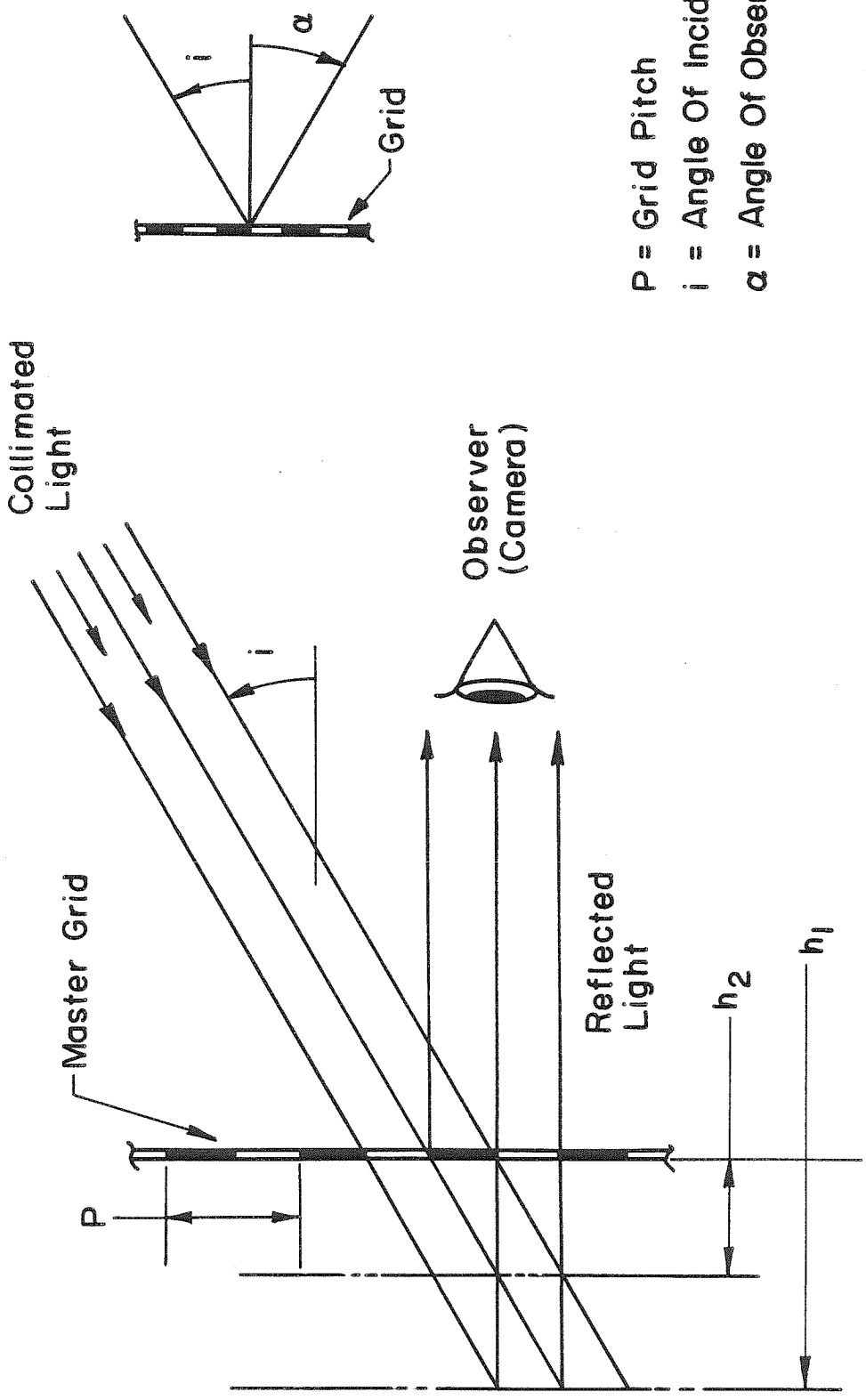

FIG. 6 OBS SCHEMATIC

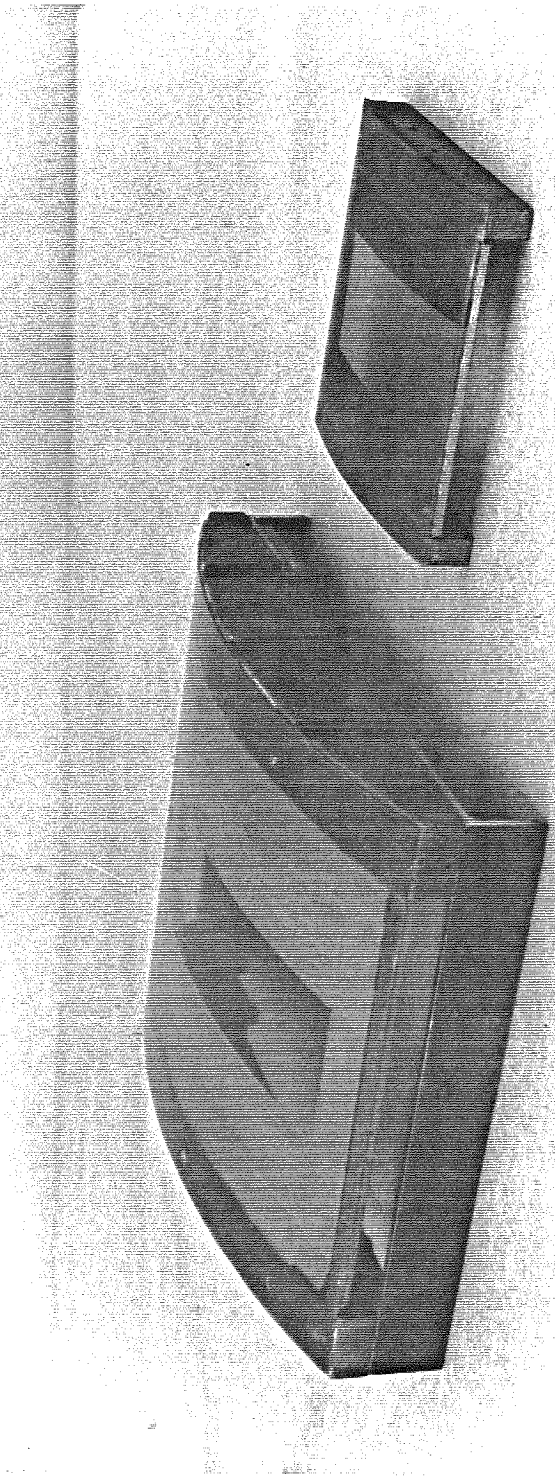

FIG. 7 CURVED MOIRÉ GRIDS

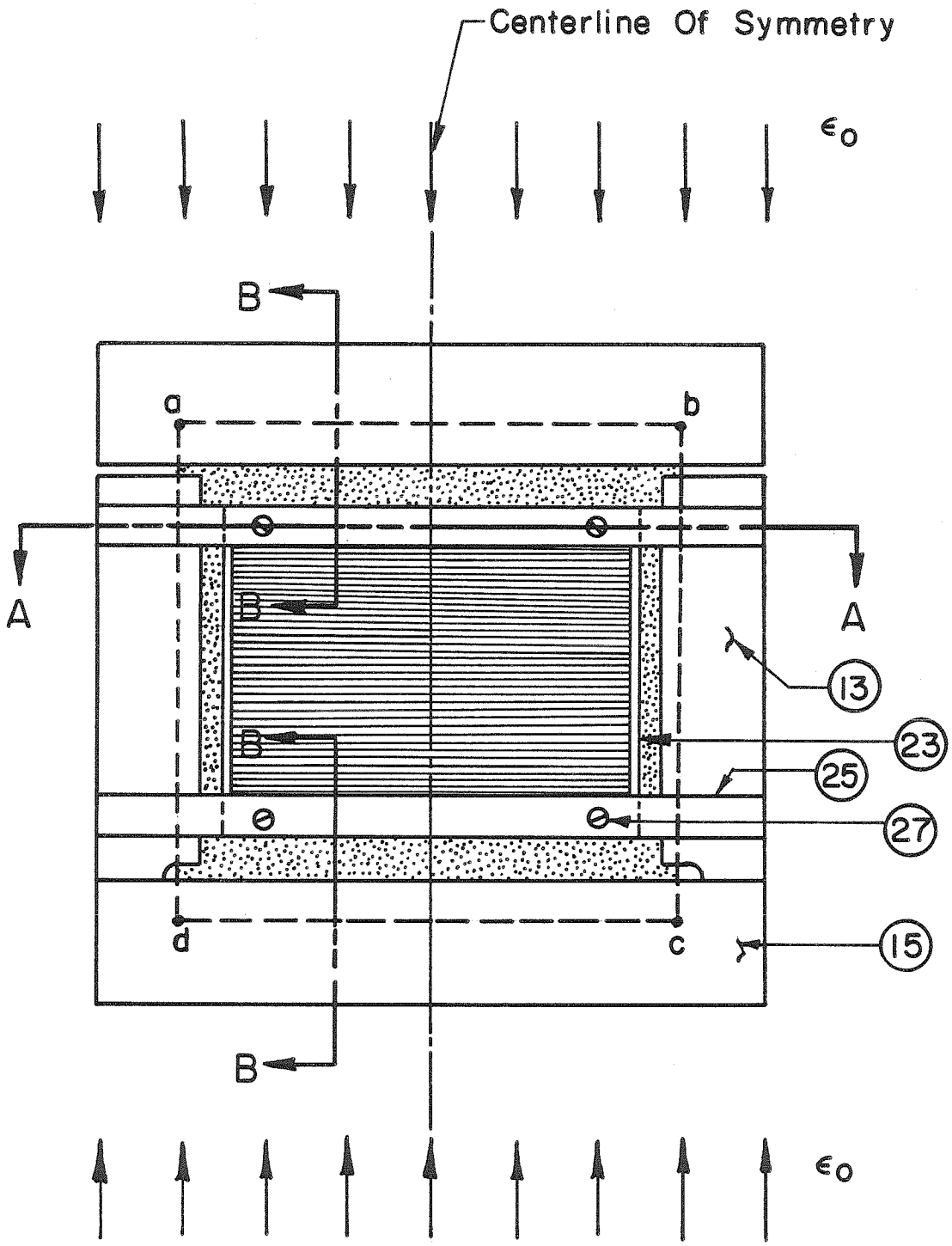

FIG. 8 FIXTURE AND GRID SCHEMATIC

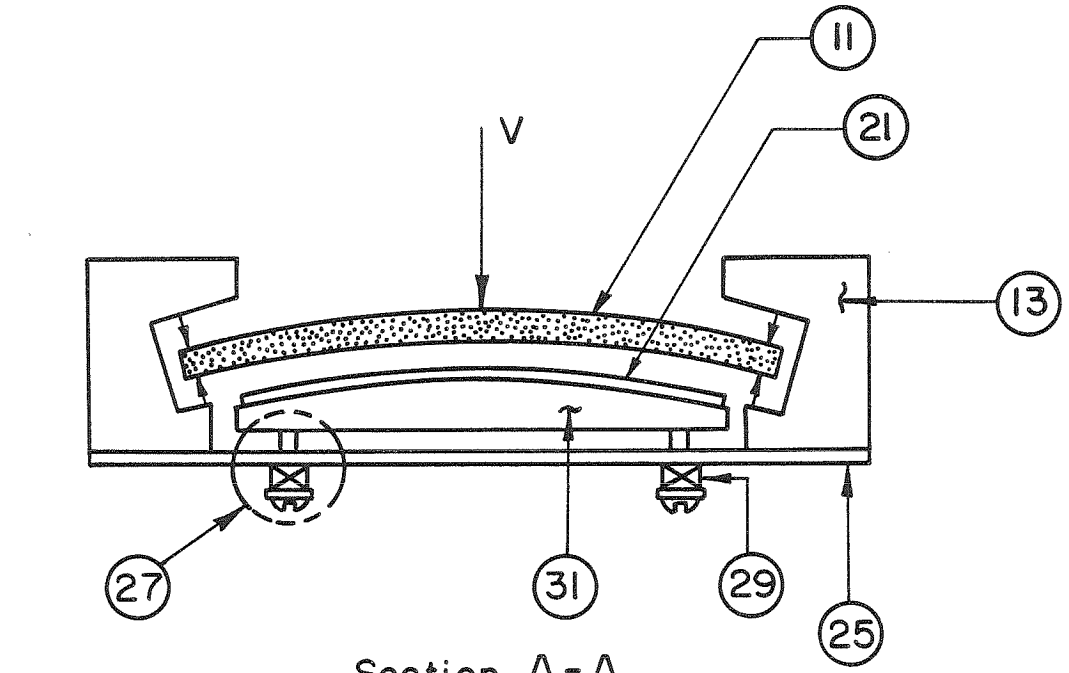

Section A-A

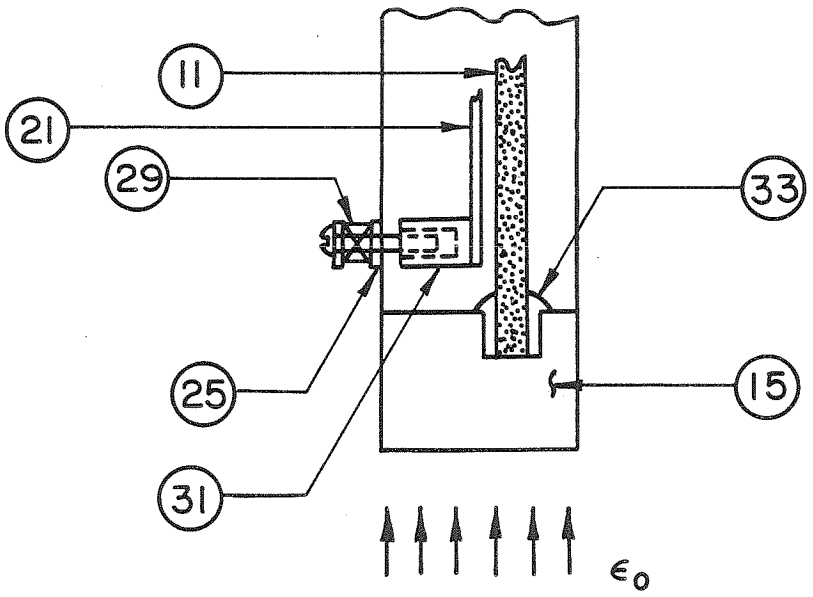

Section B-B

FIG. 9 FIXTURE AND GRID SCHEMATIC

NOTATION FOR FIGURES 8 and 9

-11	panel
-13	panel stiffener (2)
-15	loading bar (2)
-21	moiré grid
-23	grid stiffener (2)
-25	grid support (2)
-27	grid screw -spring mechanism (4)
-29	compression spring (4)
-31	grid stiffener (2)
-33	devcon
V	projectile
ε_o	applied strain
abcd	panel edge

panel

moiré grid

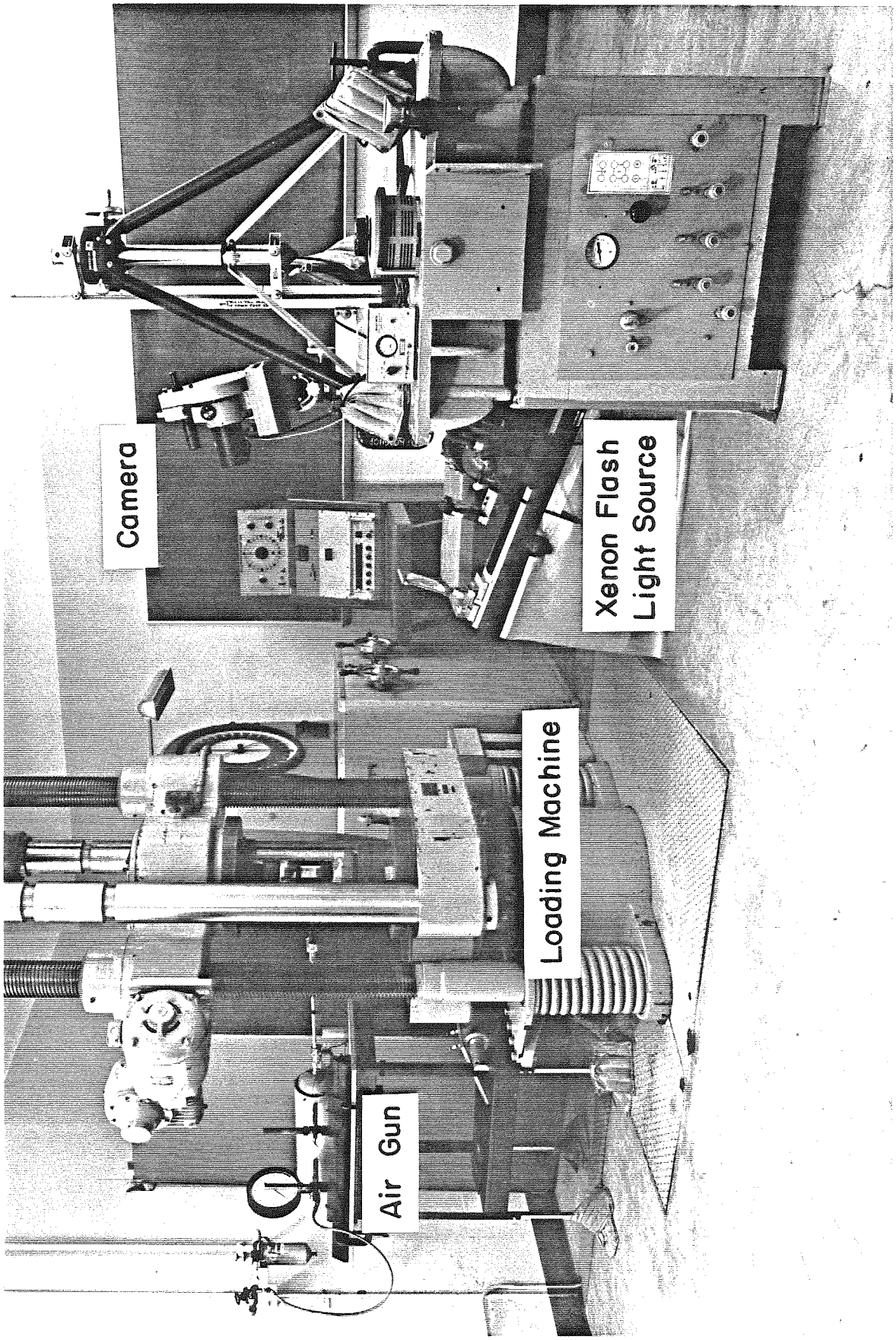

FIG.10 EXPERIMENTAL TEST SET UP

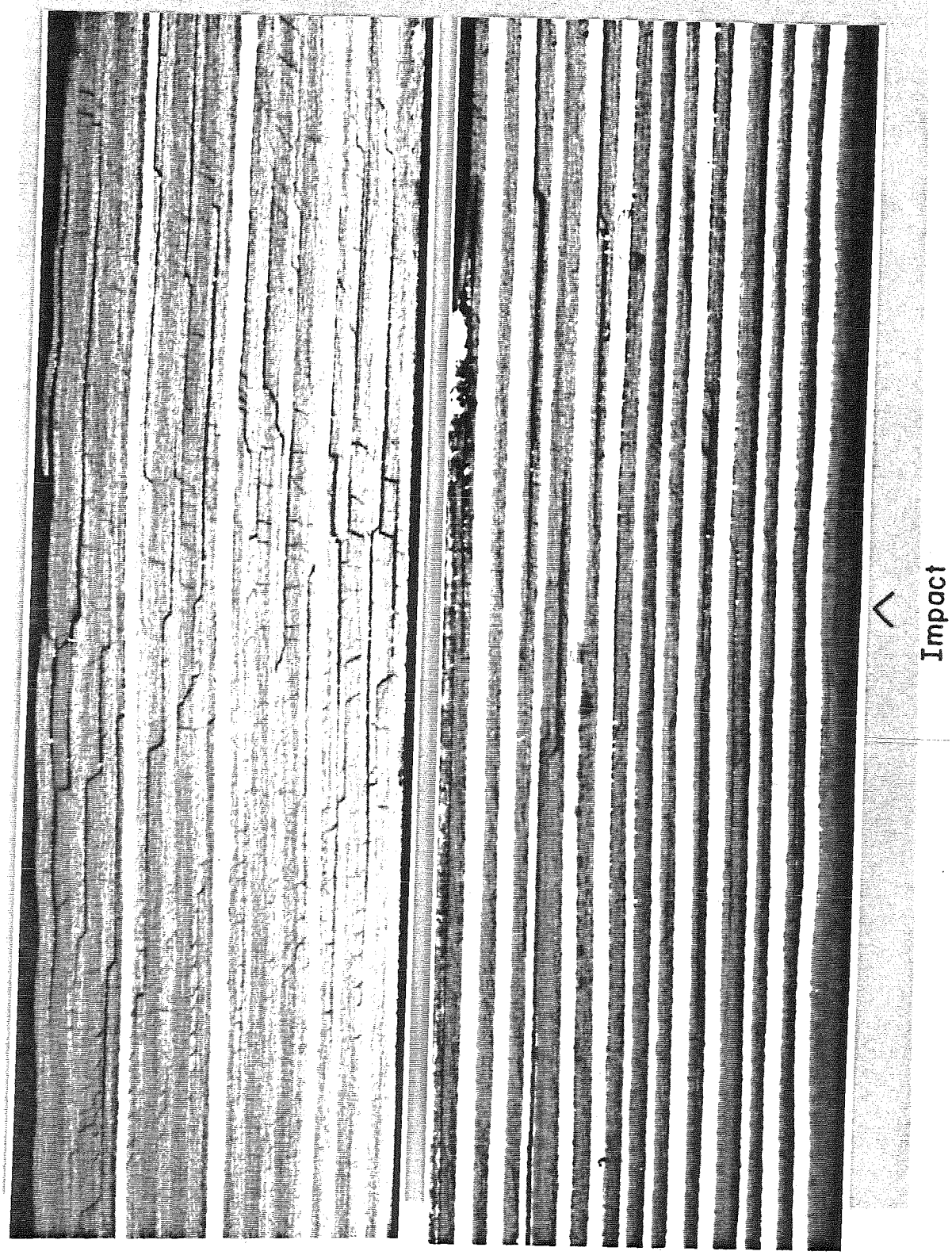

FIG. 11 INTERIOR IMPACT DAMAGE (REF. 4)

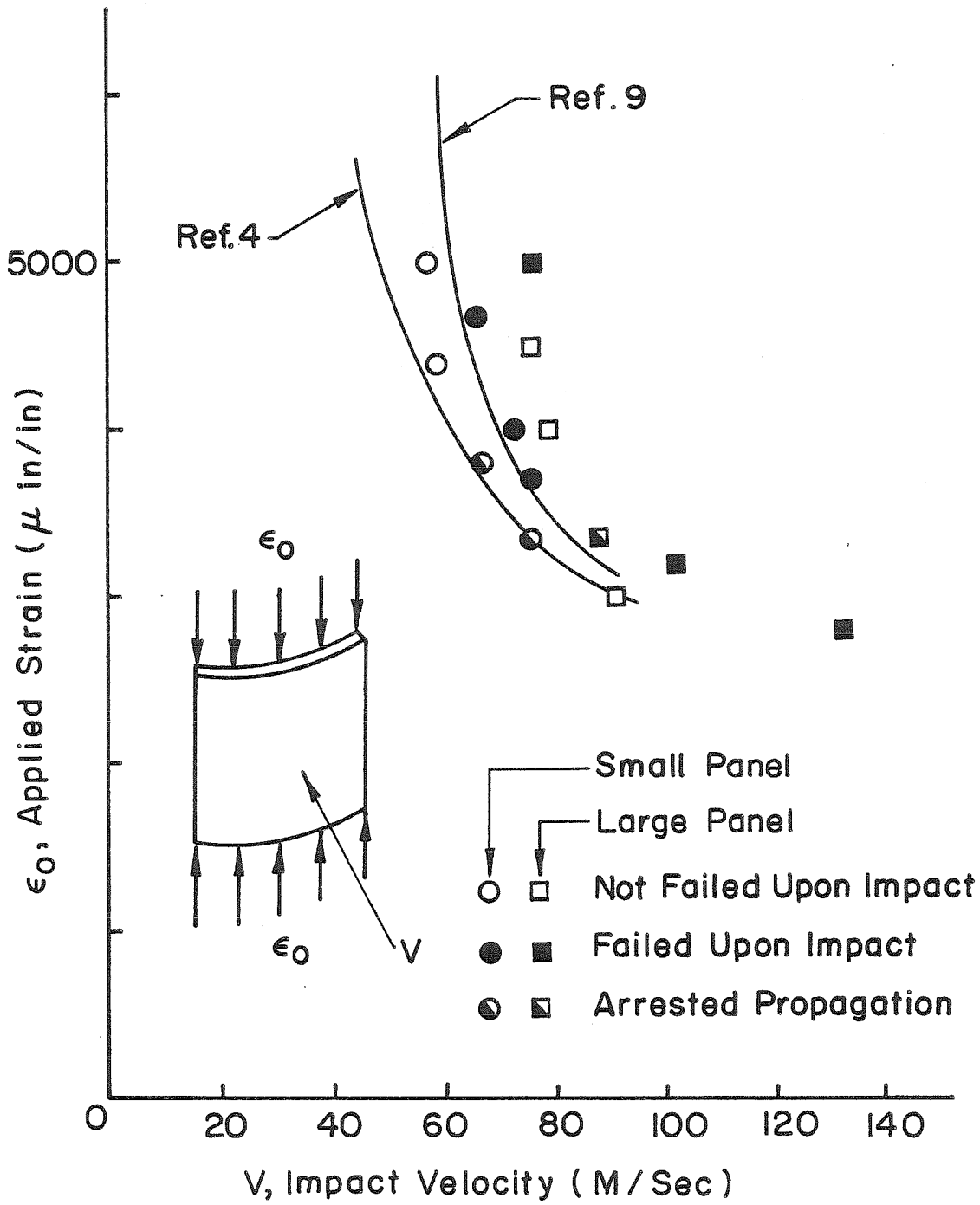

FIG. 12 THRESHOLD CURVE FOR CURVED PANELS

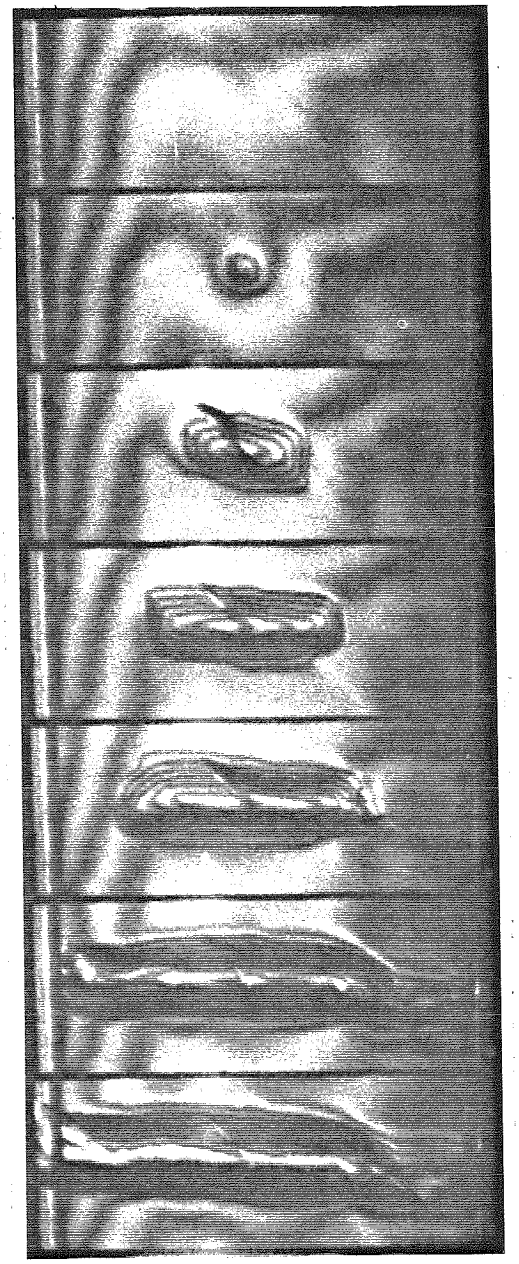

1 in.

FIG. 13 SX-1 MOIRÉ SEQUENCE

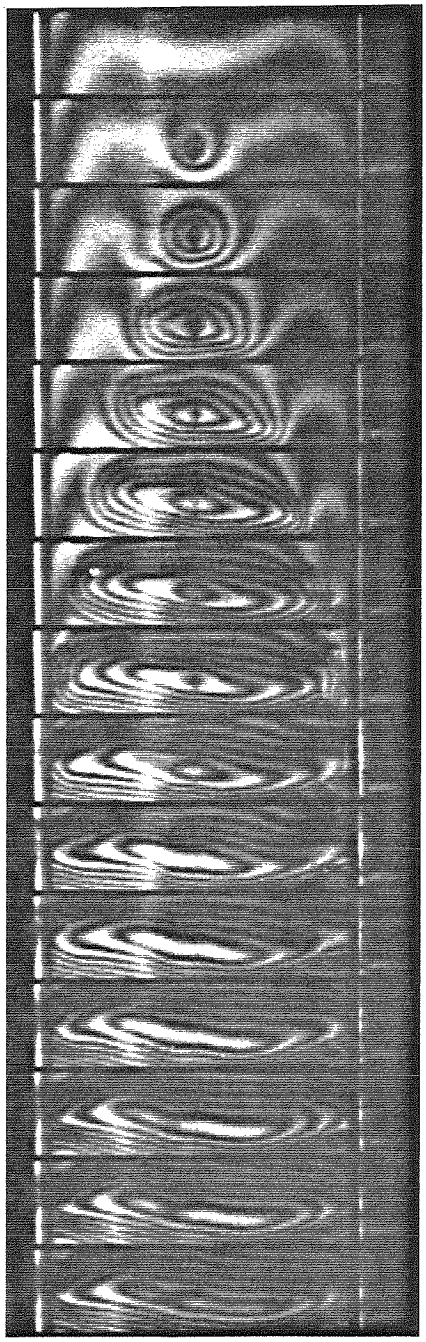

FIG. 14 SX-3 MOIRÉ SEQUENCE

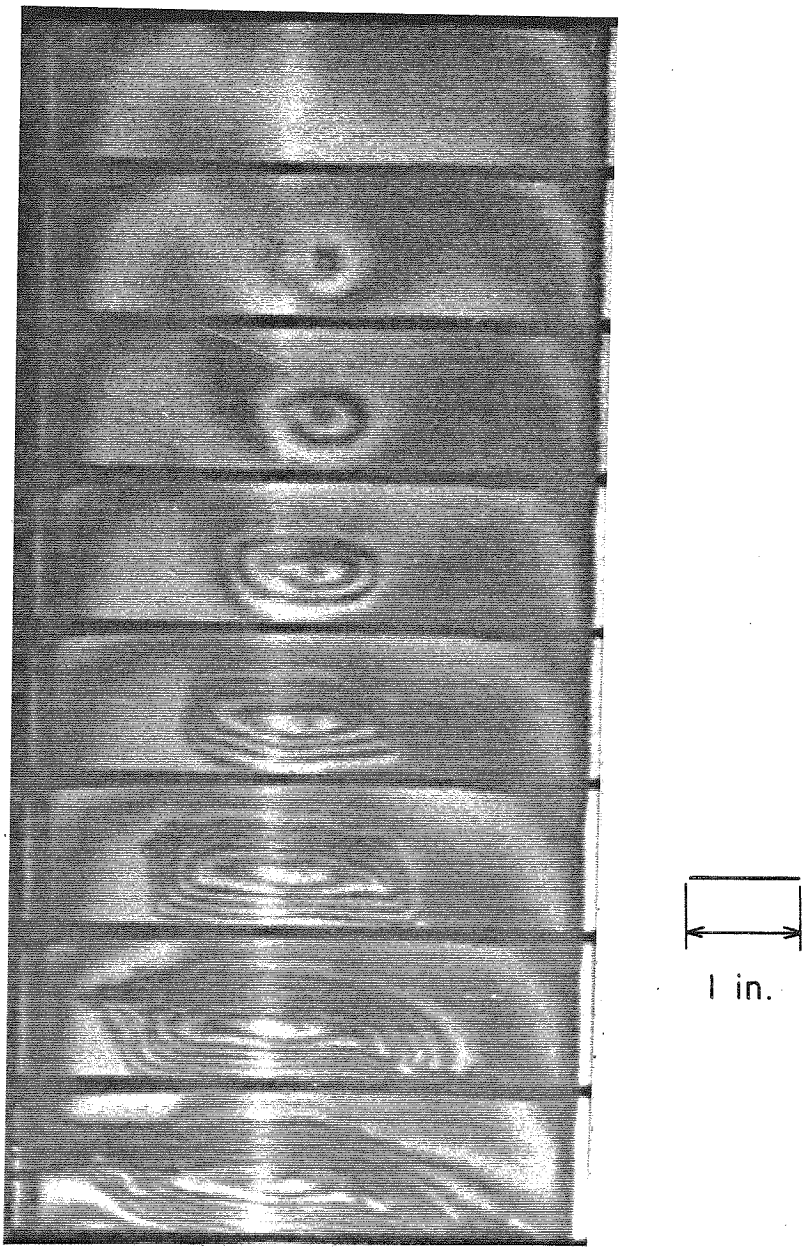

FIG. 15 SX-4 MOIRÉ SEQUENCE

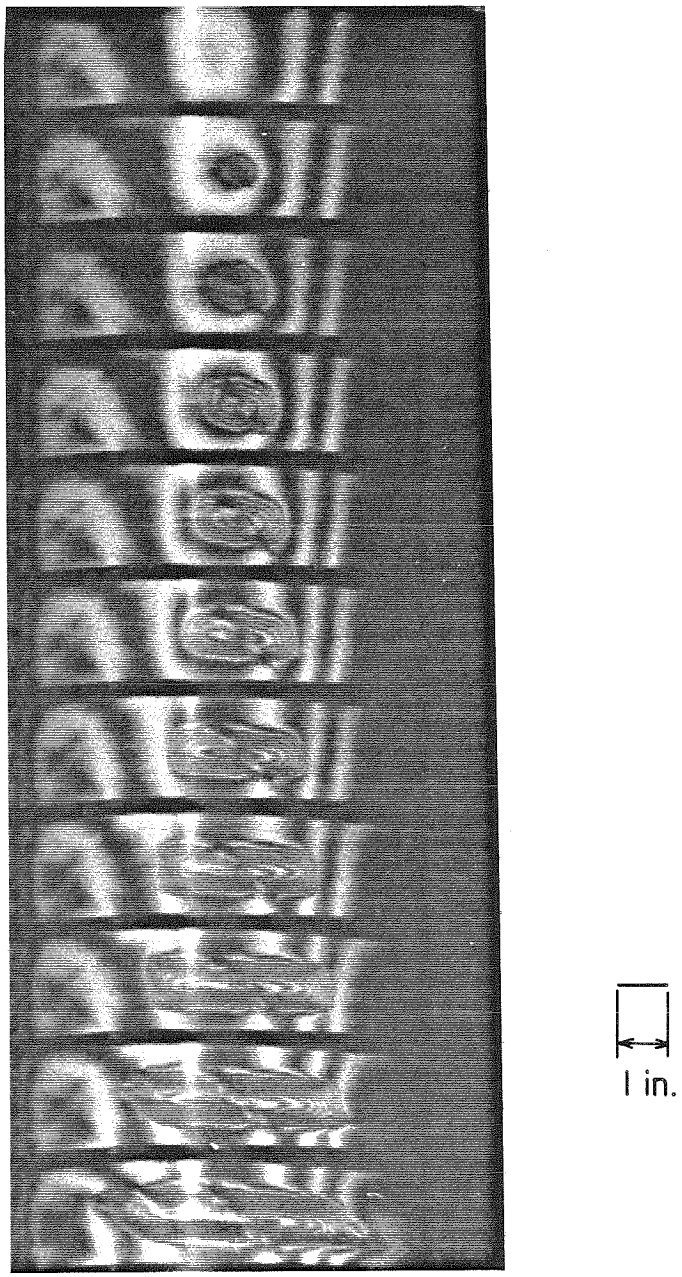

FIG. 16 X-1 MOIRÉ SEQUENCE

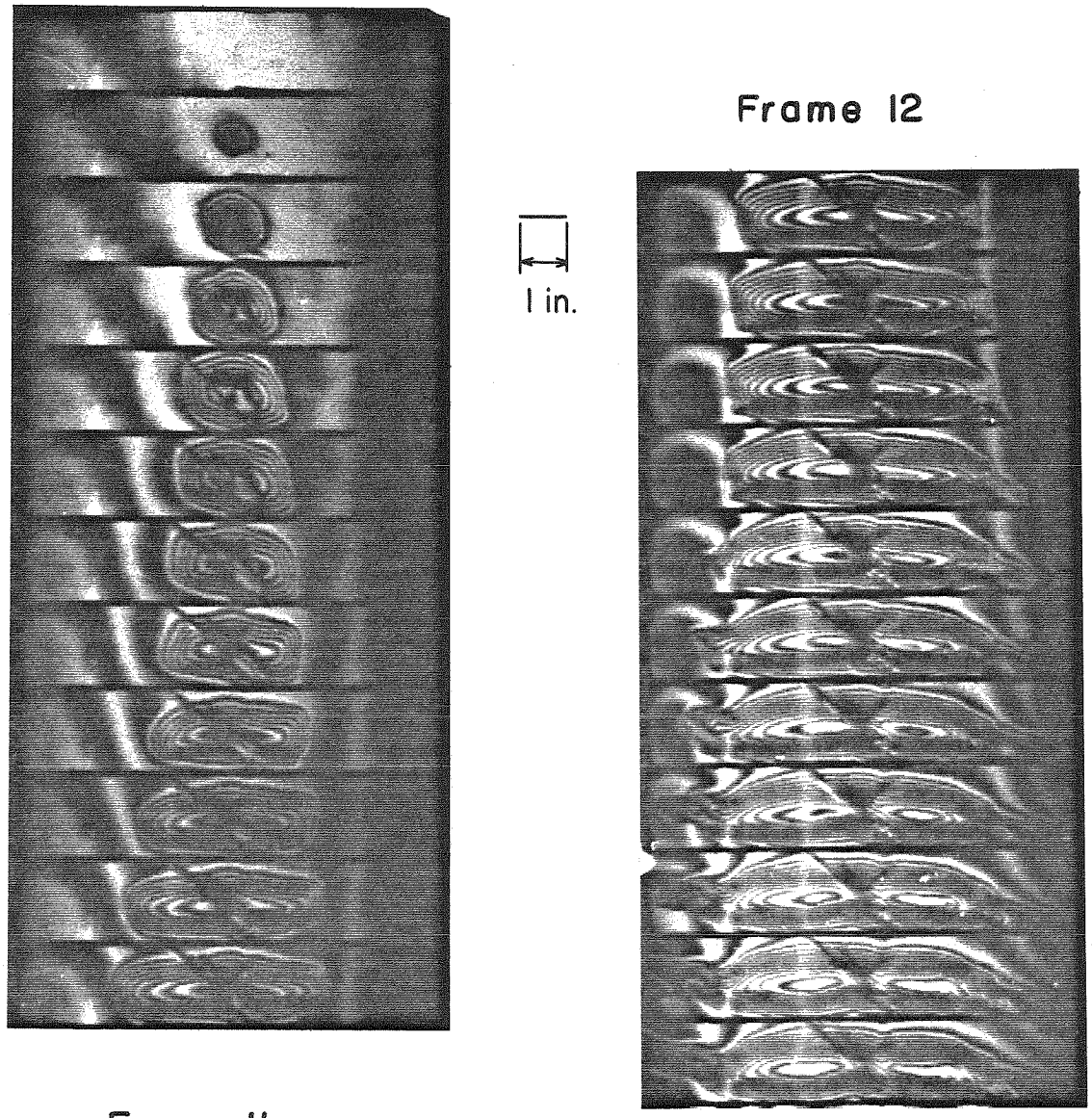

FIG. 17 X-3 MOIRÉ SEQUENCE

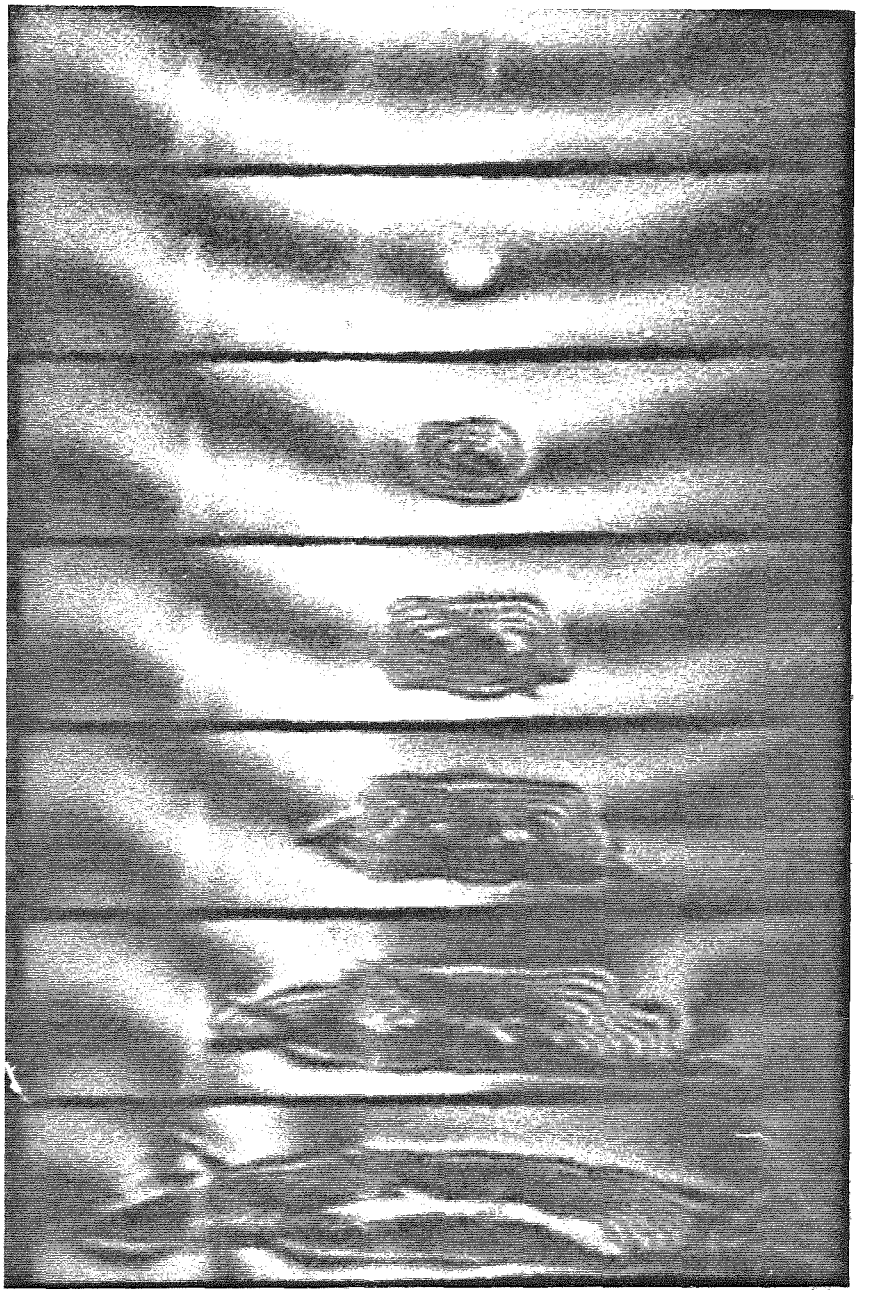

1 in.

FIG. 18 X-5 MOIRÉ SEQUENCE

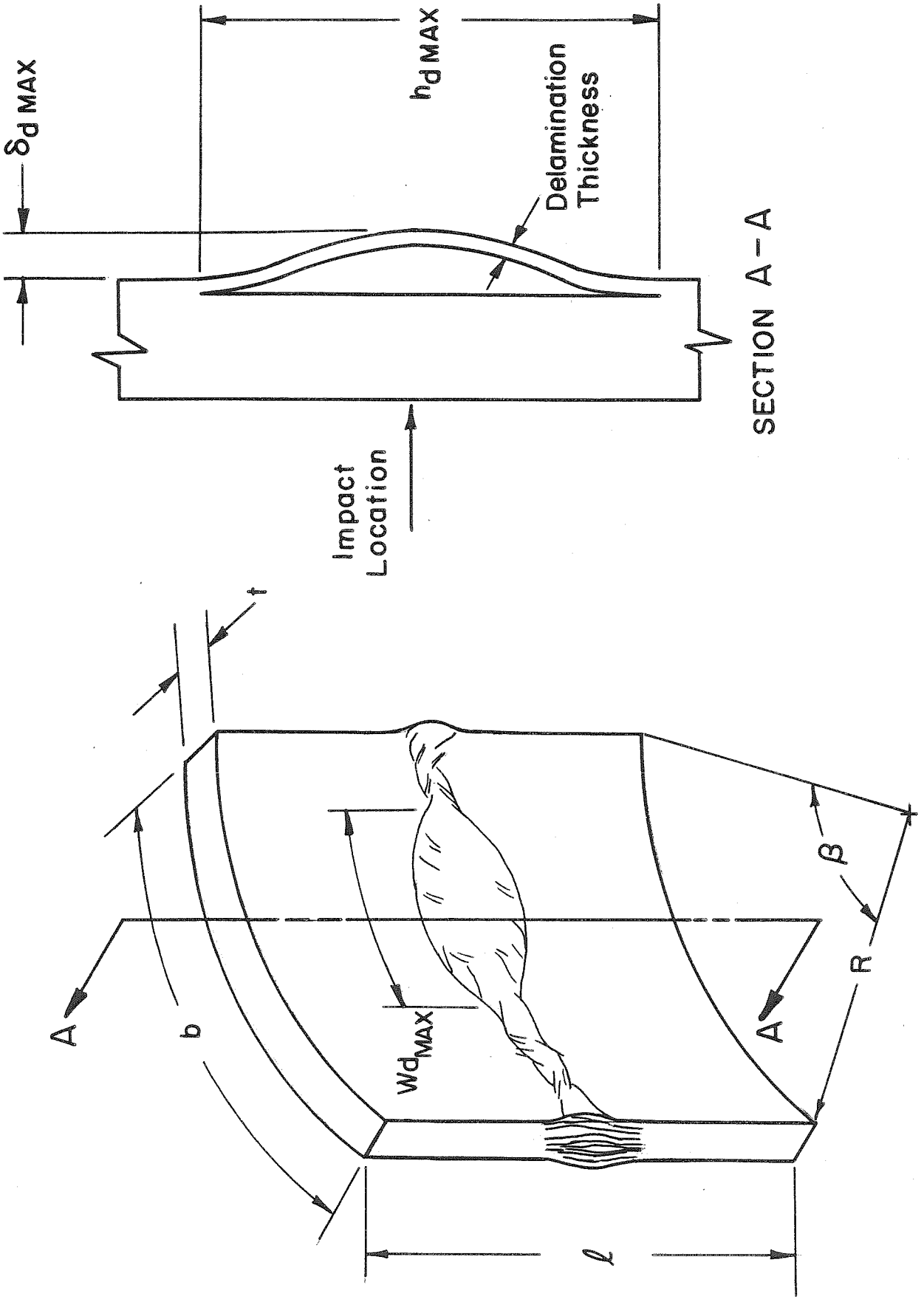

FIG. 19 PANEL SCHEMATIC

Impact face

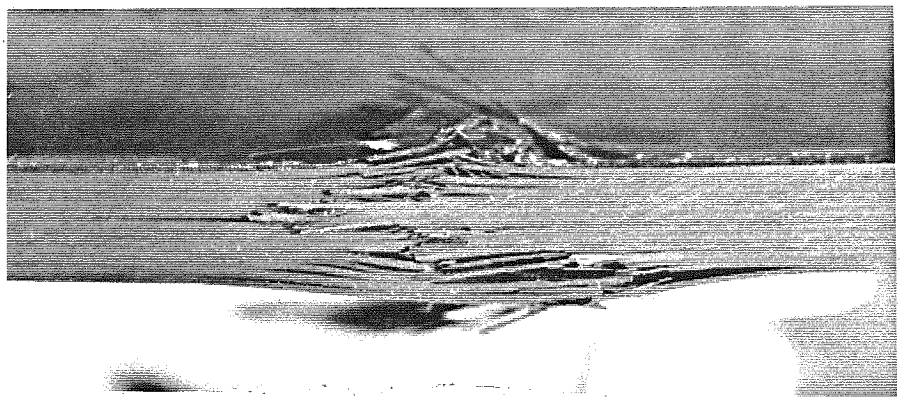

SX-4

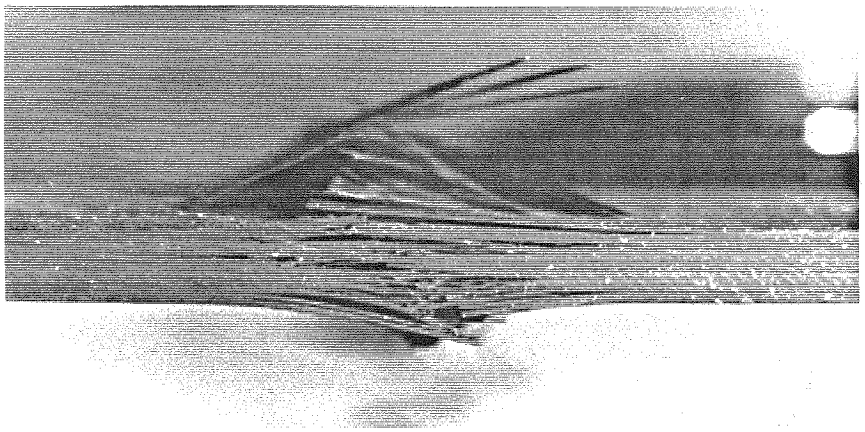

X-1

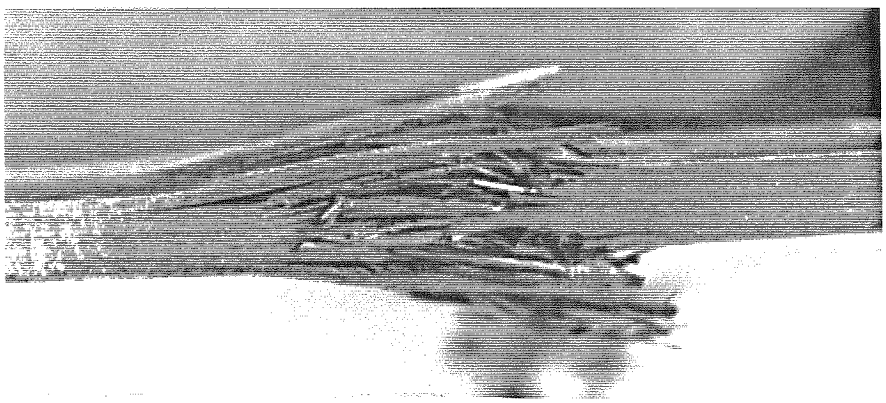

X-5

Moiré face

FIG. 20 CURVED PANEL EDGE DAMAGE

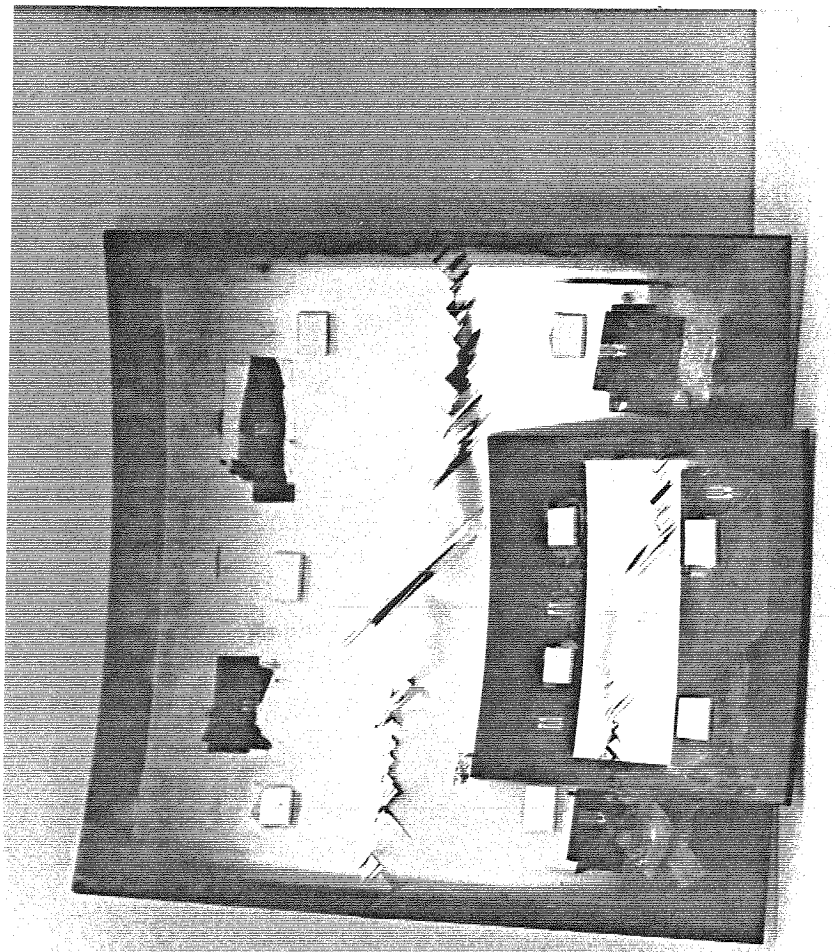

FIG. 25 X-1 AND SX-4 PANELS - MOIRÉ FACE

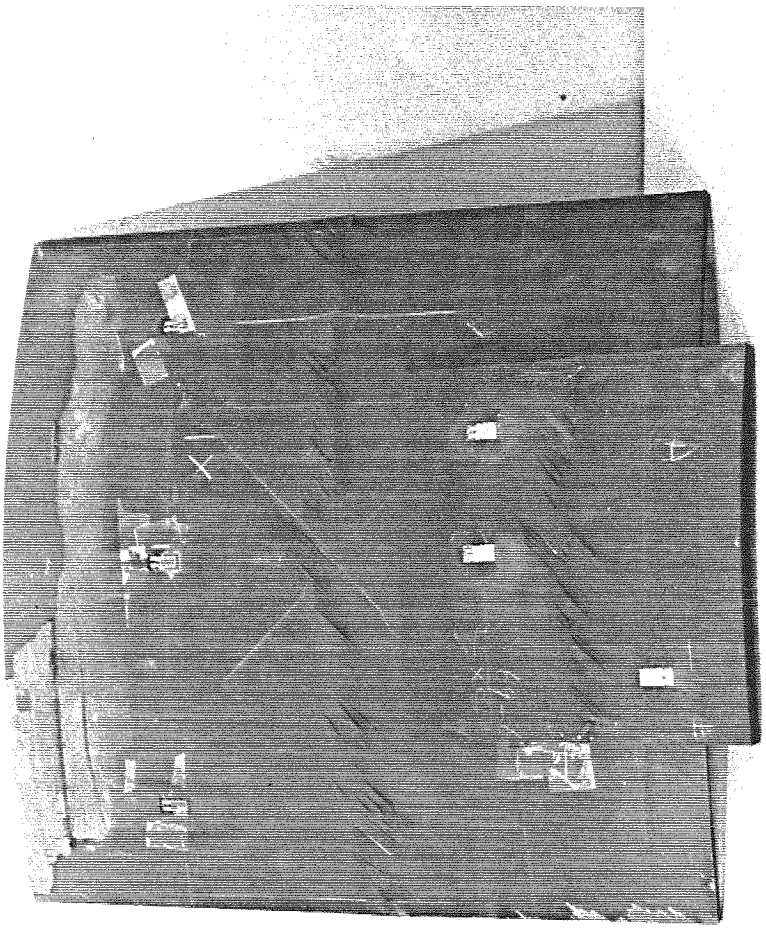

FIG. 26 X-1 AND SX-4 PANELS - IMPACT FACE

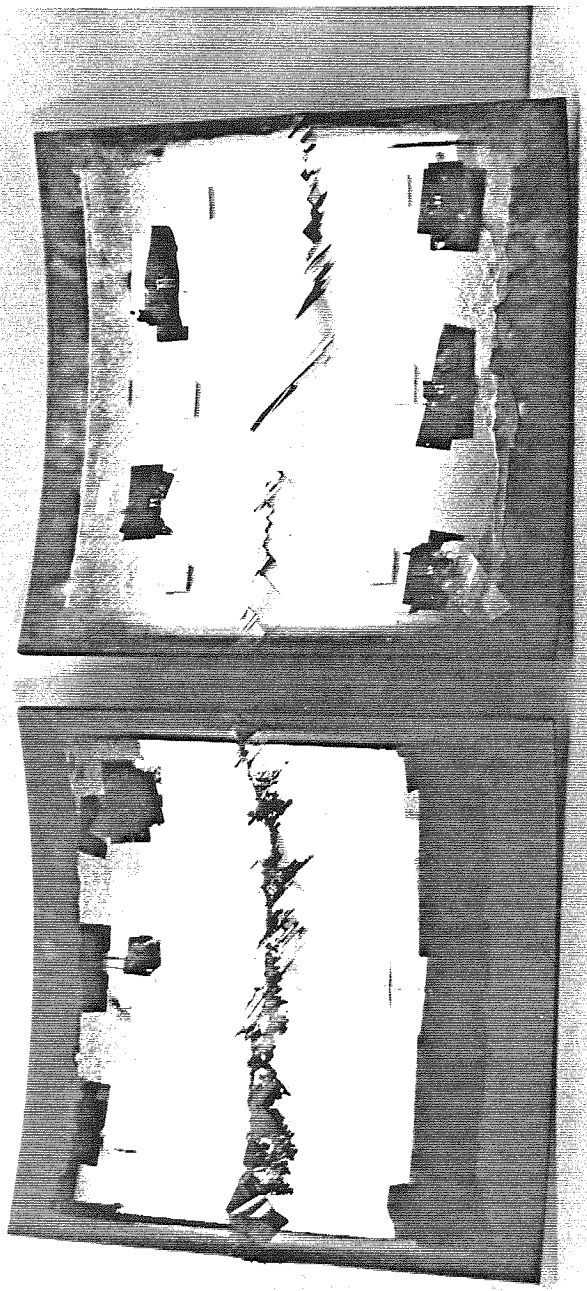

FIG. 27 X-5 AND X-1 PANELS - MOIRÉ FACE

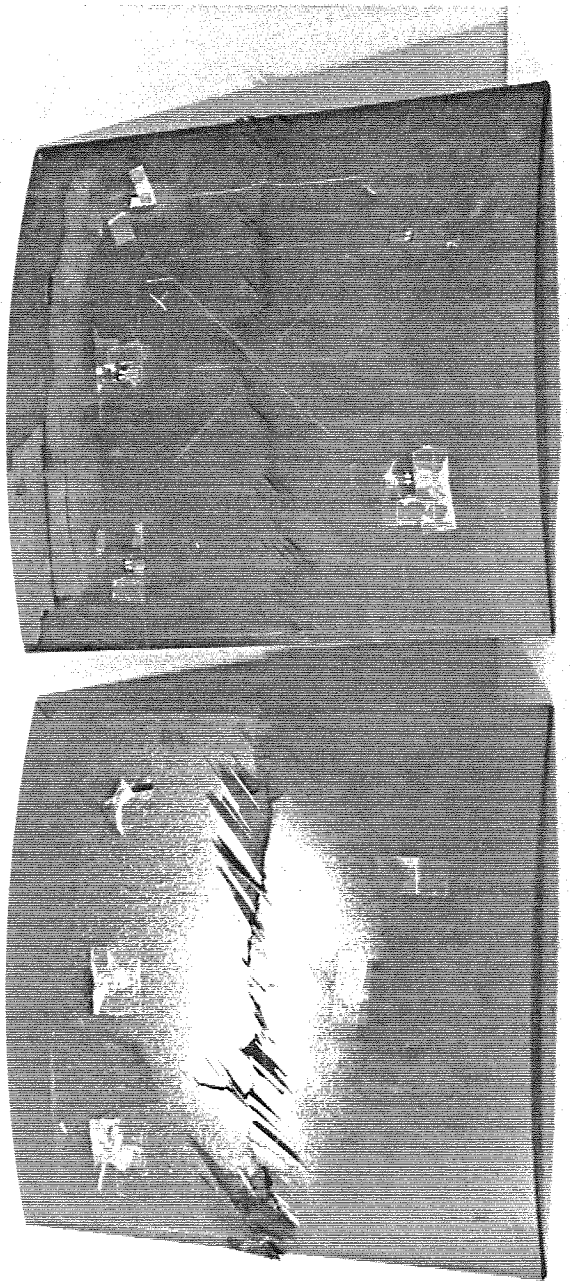

FIG. 28 X-5 AND X-1 PANELS - IMPACT FACE

Table 2

Test	ϵ_o	W_{dMax}	h_{dMax}
X-3	2800	5.50	1.92
X-1	3167	4.02	1.30
SX-3	3667	3.92	1.60
SX-1	4000	2.23	.96
SX-4	4667	2.30	.98
X-5	5000	1.96	1.04

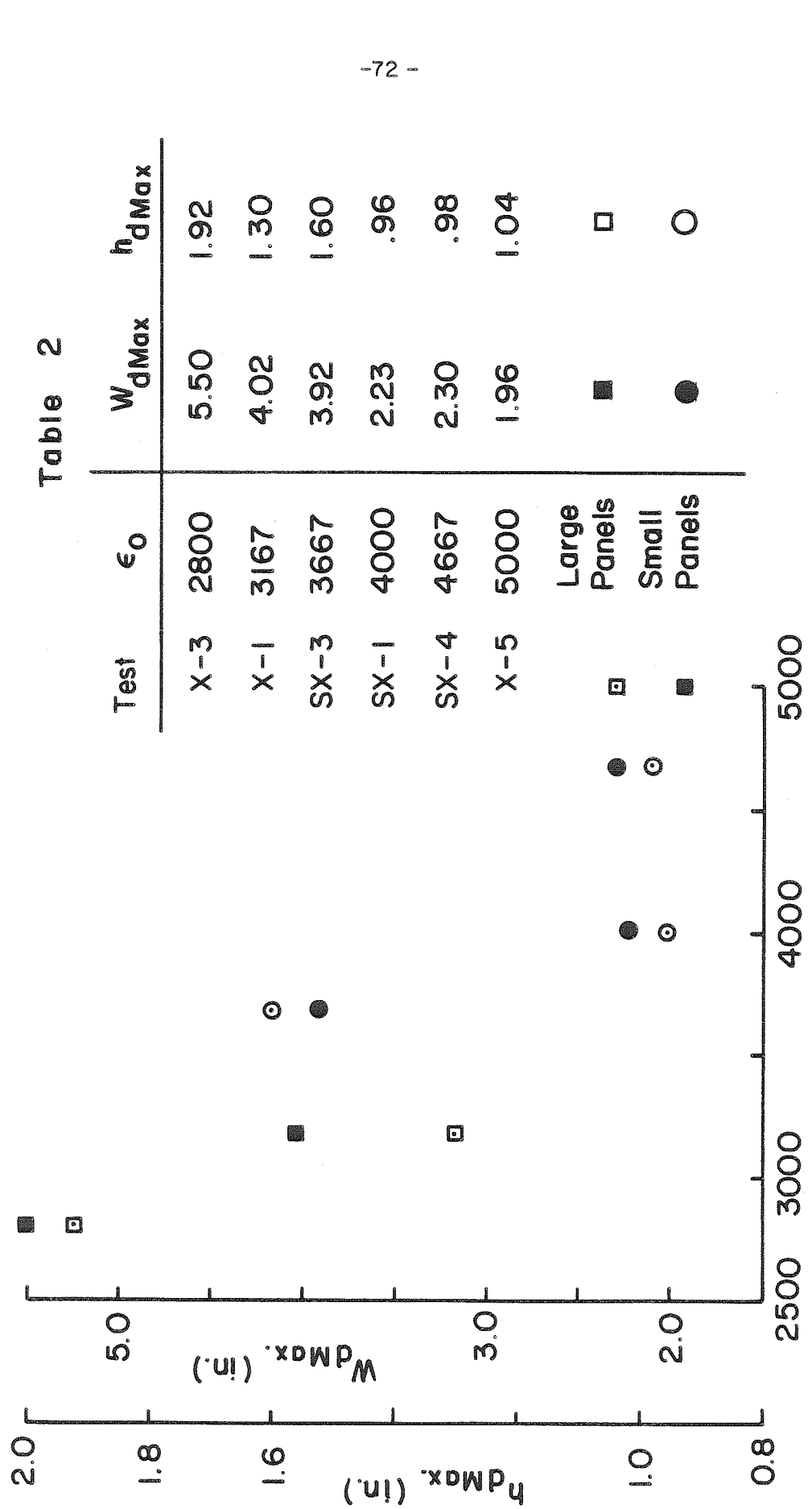

FIG. 29 $W_{dMAX.}$ AND $h_{dMAX.}$ VS ϵ_o

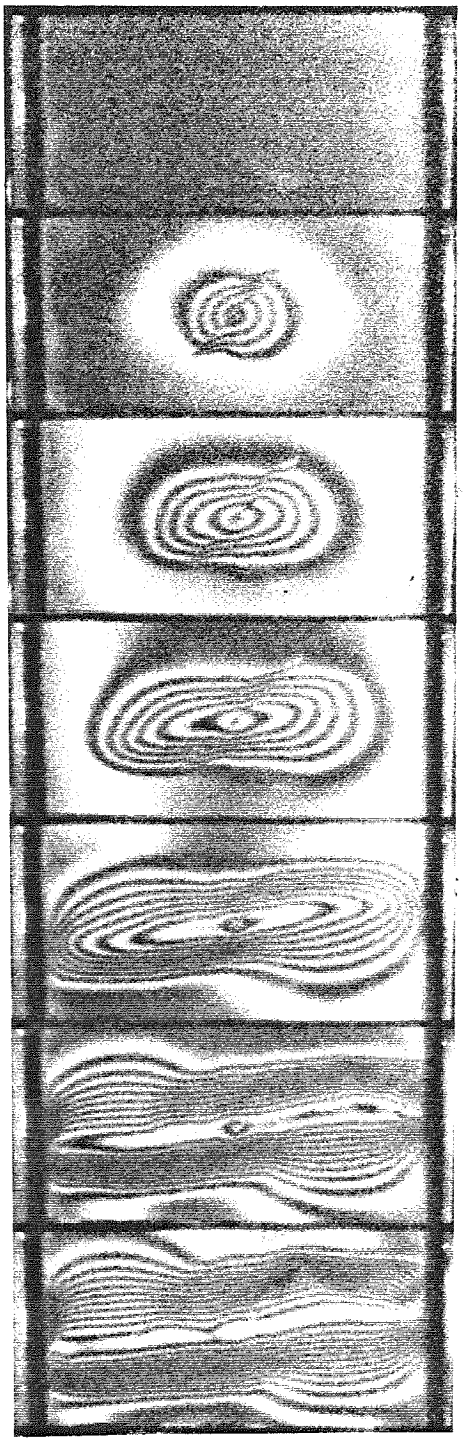

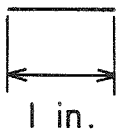

FIG. 30 FLAT PANEL MOIRÉ SEQUENCE
(REF. 4)

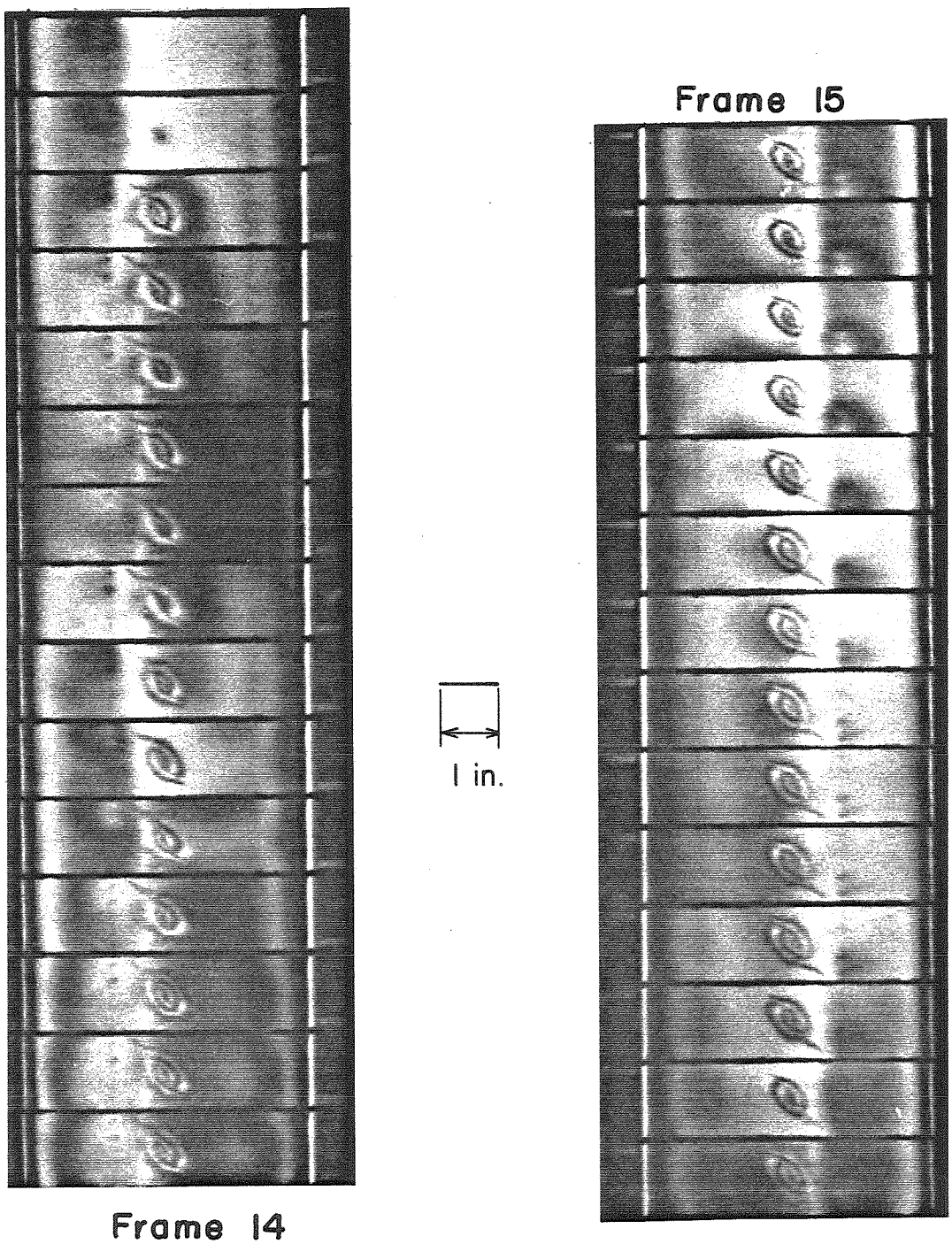

FIG.31 SX-2 MOIRÉ SEQUENCE

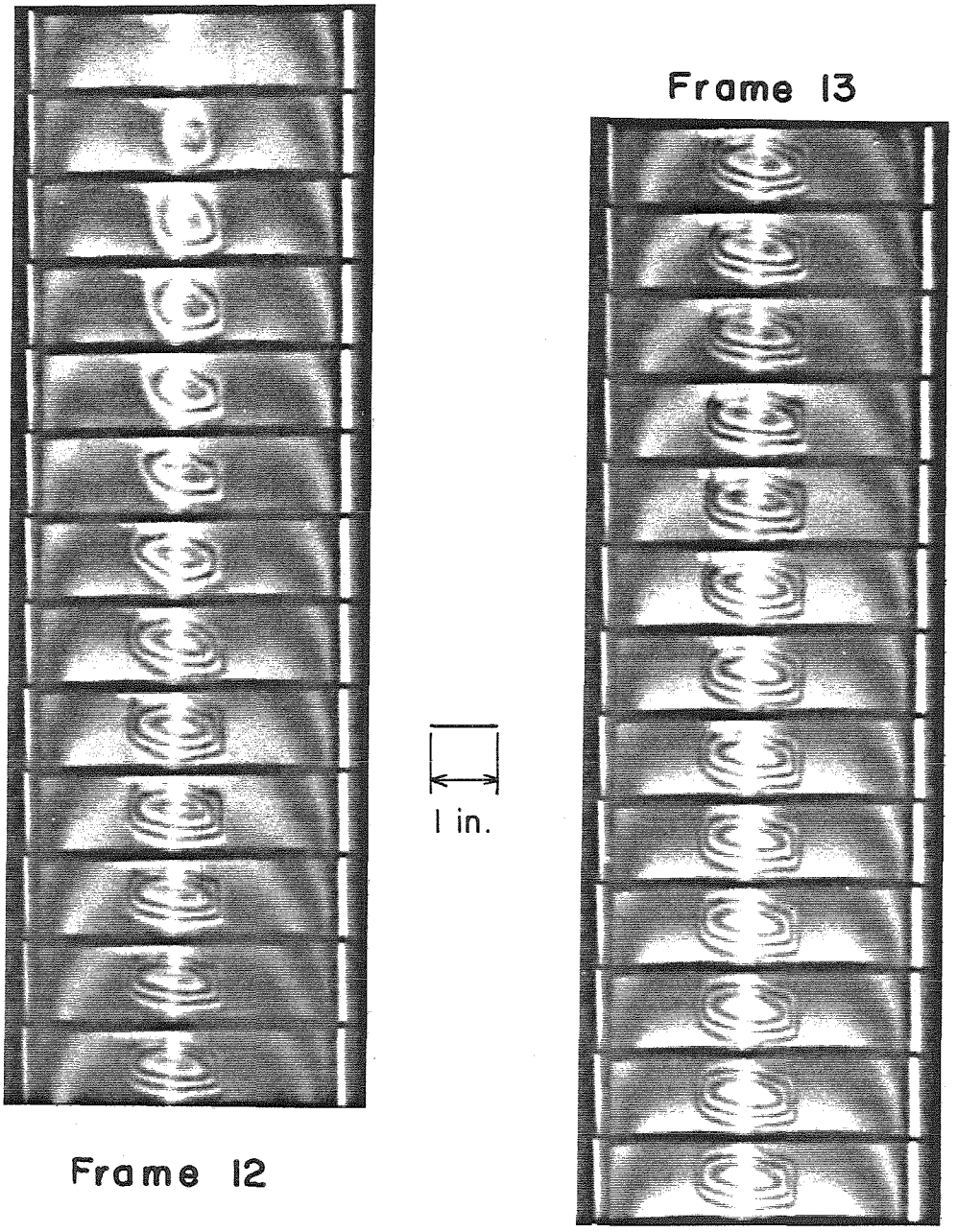

FIG. 32 SX-5 MOIRÉ SEQUENCE

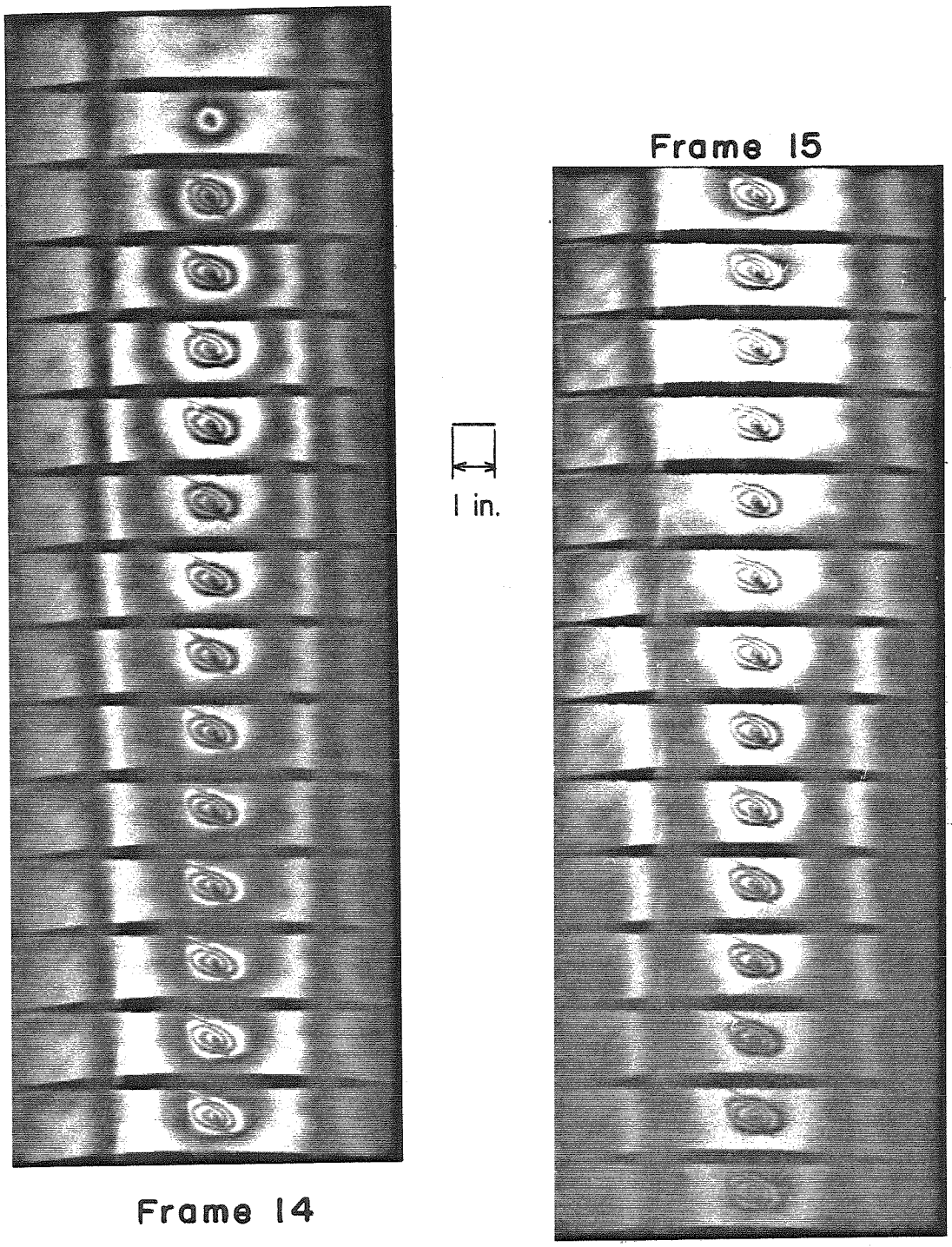

FIG. 33 X - 6 MOIRÉ SEQUENCE

TABLE 3 - SUMMARY OF EXPERIMENTAL DATA

Test #	ε_o	V	Failure Mode	f	Δt	V_p	W_dMax	δ_dMax	b_i
SX-1	4000	73	F	.0175	50	640	2.23	0.116	0.77
SX-2	3333	76	B	.0165	27		0.70	0.050	0.70
SX-3	3667	76	F	.0165	30.8	900	3.92	0.132	0.89
SX-4	4667	66	F	.0220	26.7	670	2.30	0.132	0.64
SX-5	3800	67	AP	.0220	27.8		1.50	0.088	0.82
SX-6	4433	60	NF	.0220					
SX-7	5000	59	NF	.0164					
X-1	3167	104	F	.0168	26.3	720	4.02	0.134	0.80
X-2	3000	92	NF	.0168					
X-3	2800	132	F	.0171	25.0	664	5.50	0,170	0.92
X-4	4000	72	NF	.0171					
X-4.5	4500	70	NF	.0171					
X-5	5000	70	F	.0171	25.7	1050	1.96	0.120	0.60
X-6	3333	89	AP	.0171	26.0		1.40	0.060	0.83

NOTATION FOR TABLE 3

SX-n	Small panel test designation
X-n	Large panel test designation
ε_o	Applied strain (μin/in)
V	Impact velocity (m/sec)
F	Failed upon impact
B	Buckled delamination without propagation
AP	Buckled delamination with arrested propagation
NF	No failure upon impact
f	Moiré fringe constant (in.)
Δ t	Camera timescale (μsec)
V_p	Delamination propagation velocity (ft/sec)
W_d Max.	Maximum delamination width (in.)
δ_d Max.	Maximum out-of-plane displacement for delamination (in.)
b_i	Initial delamination diameter (in.)

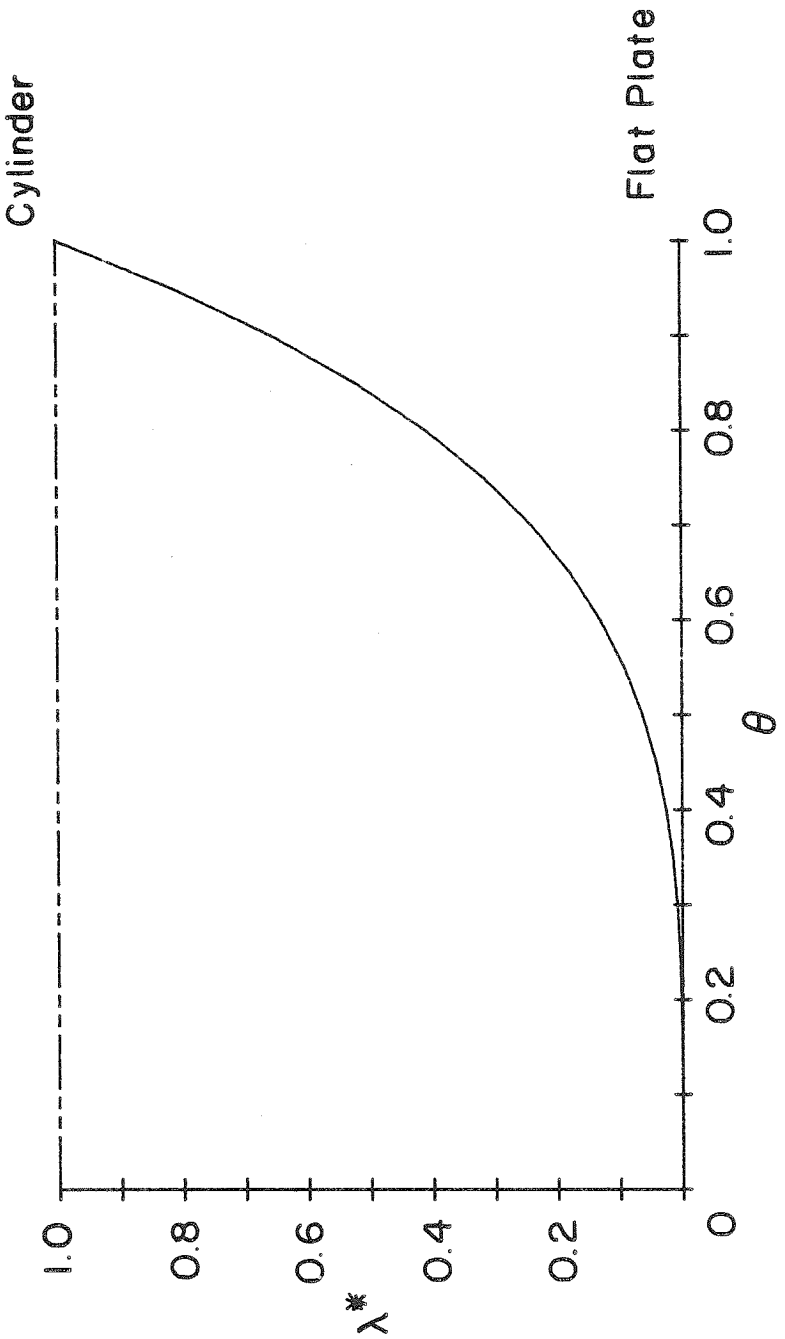

FIG. 30 λ^* VS. θ

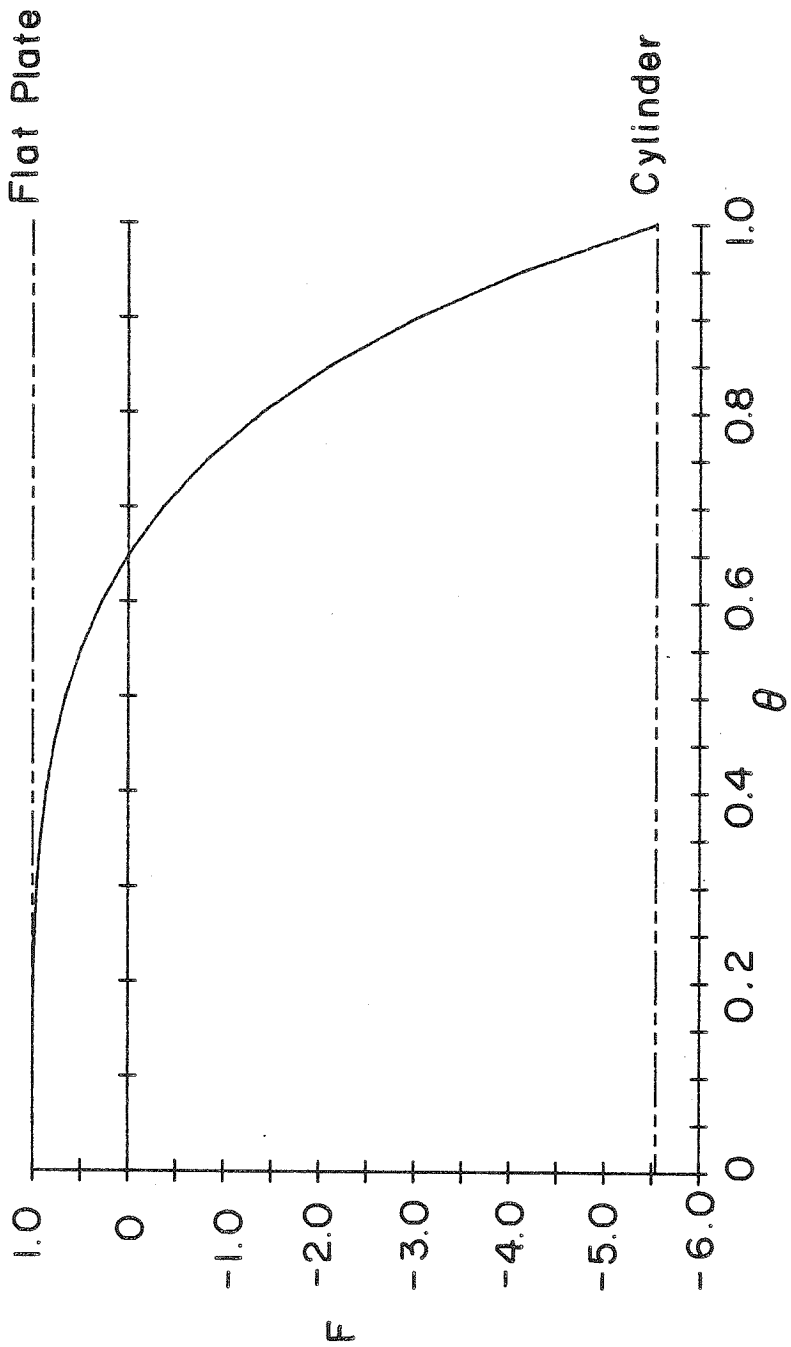

FIG. 31 F VS. θ

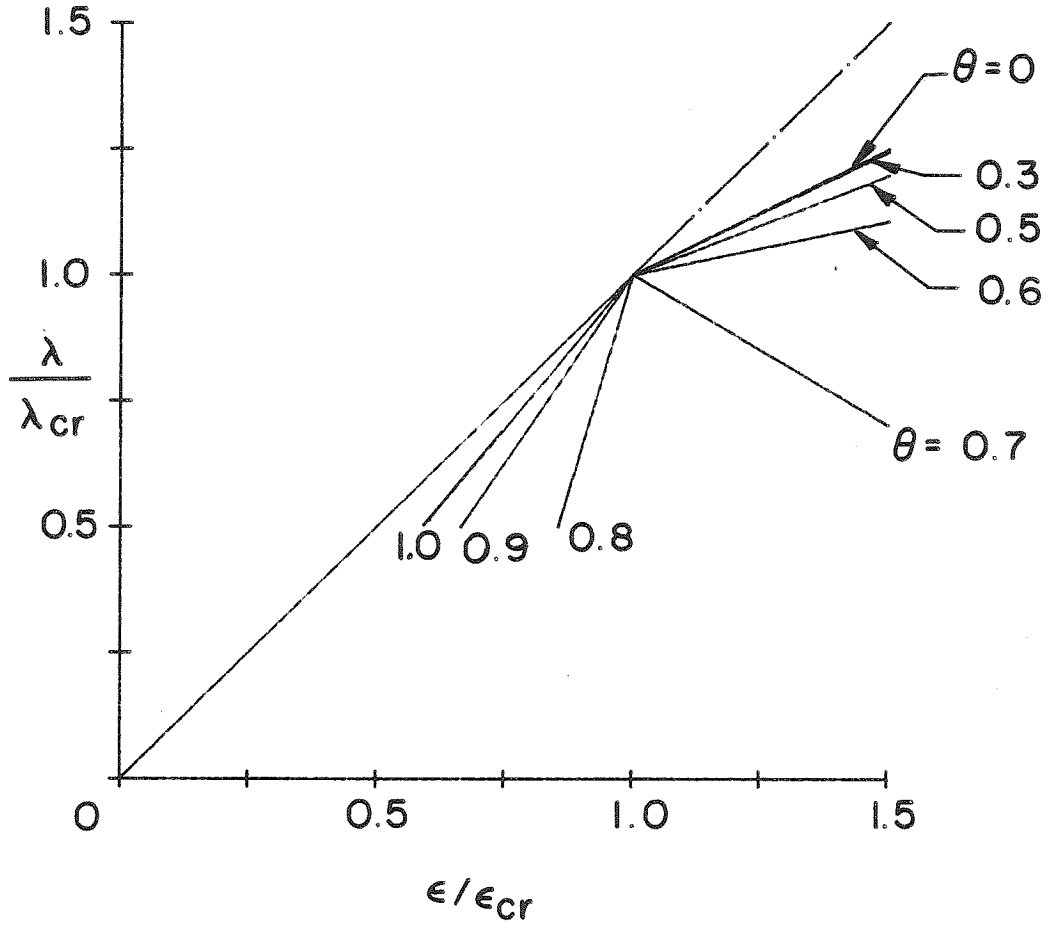

FIG. 32 λ/λ_{cr} VS. ϵ/ϵ_{cr}

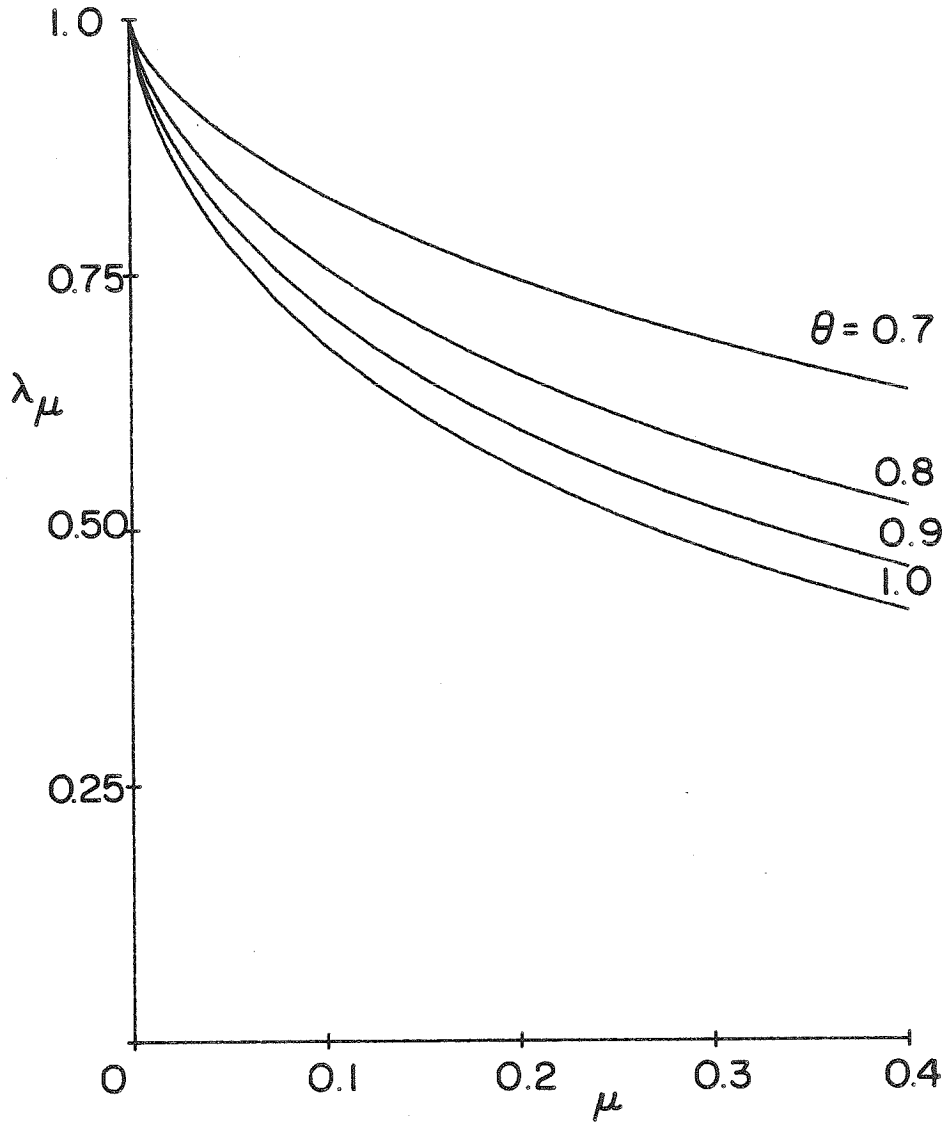

FIG. 33 λ_μ VS. μ

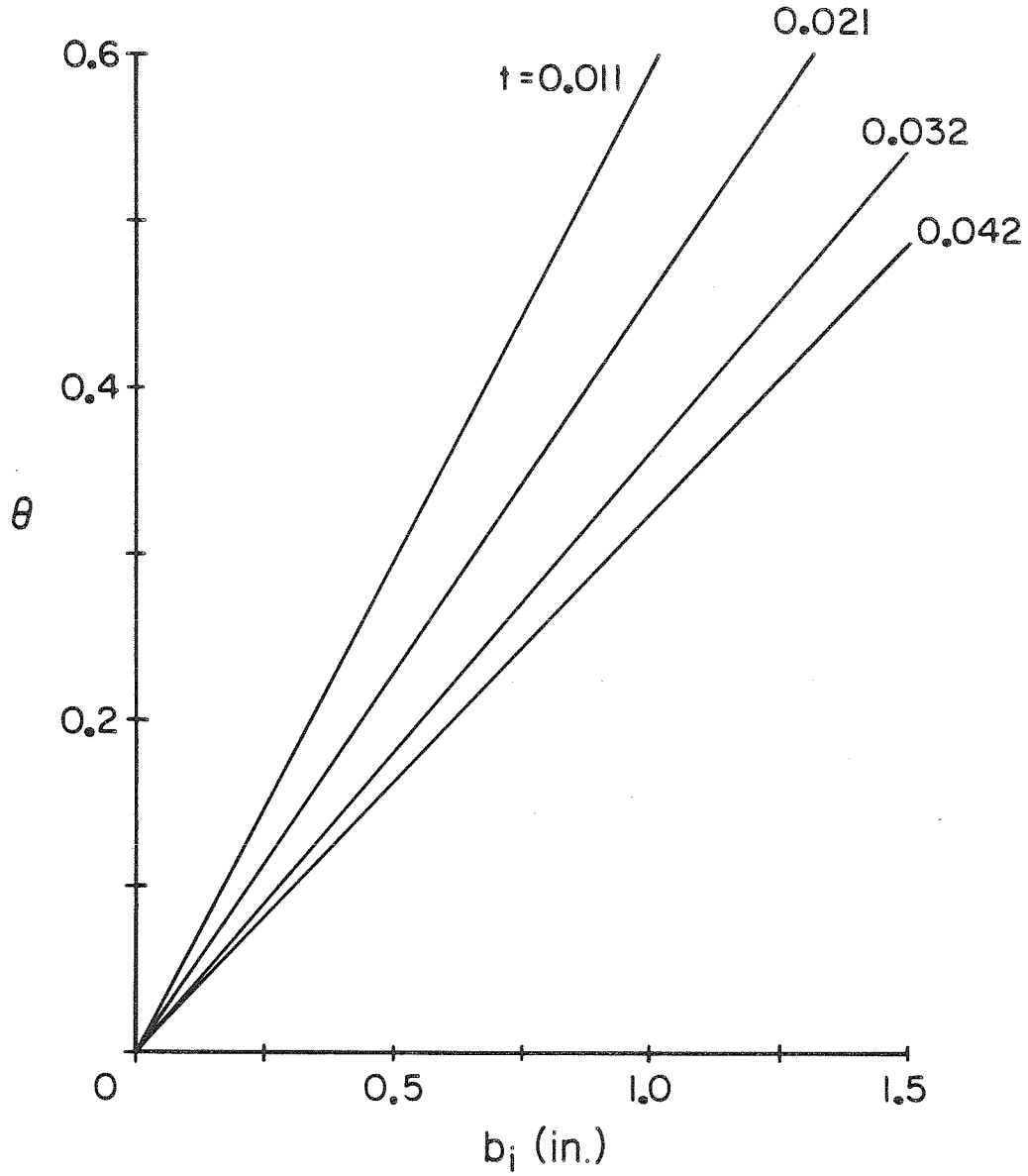

FIG. 34 θ vs. b_i

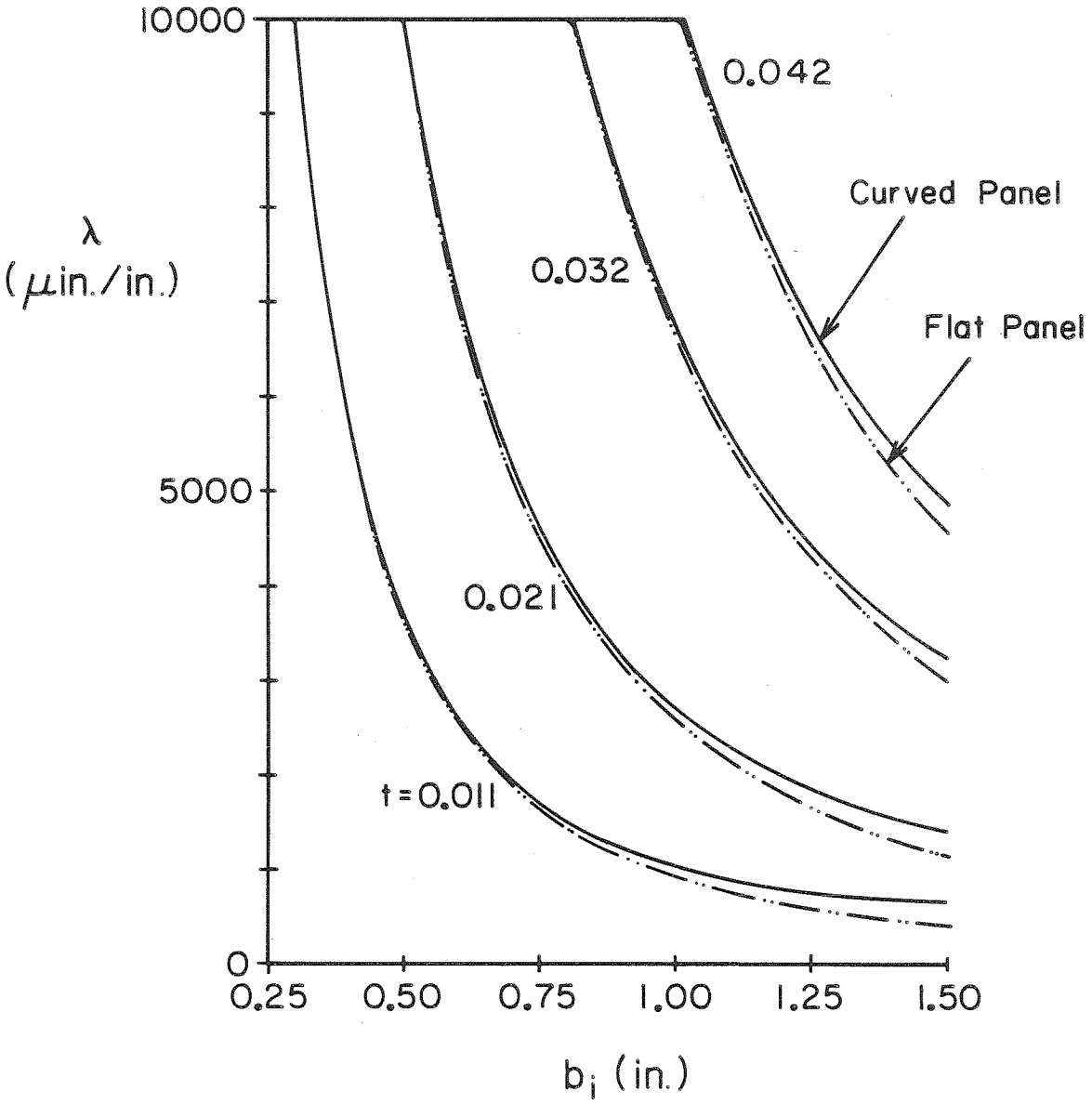
10000
5000
0
λ
(μin./in.)
0.042
0.032
0.021
t=0.011
Curved Panel
Flat Panel
0.25
0.50
0.75
1.00
1.25
1.50
b_i (in.)

FIG. 35 λ vs. b_i

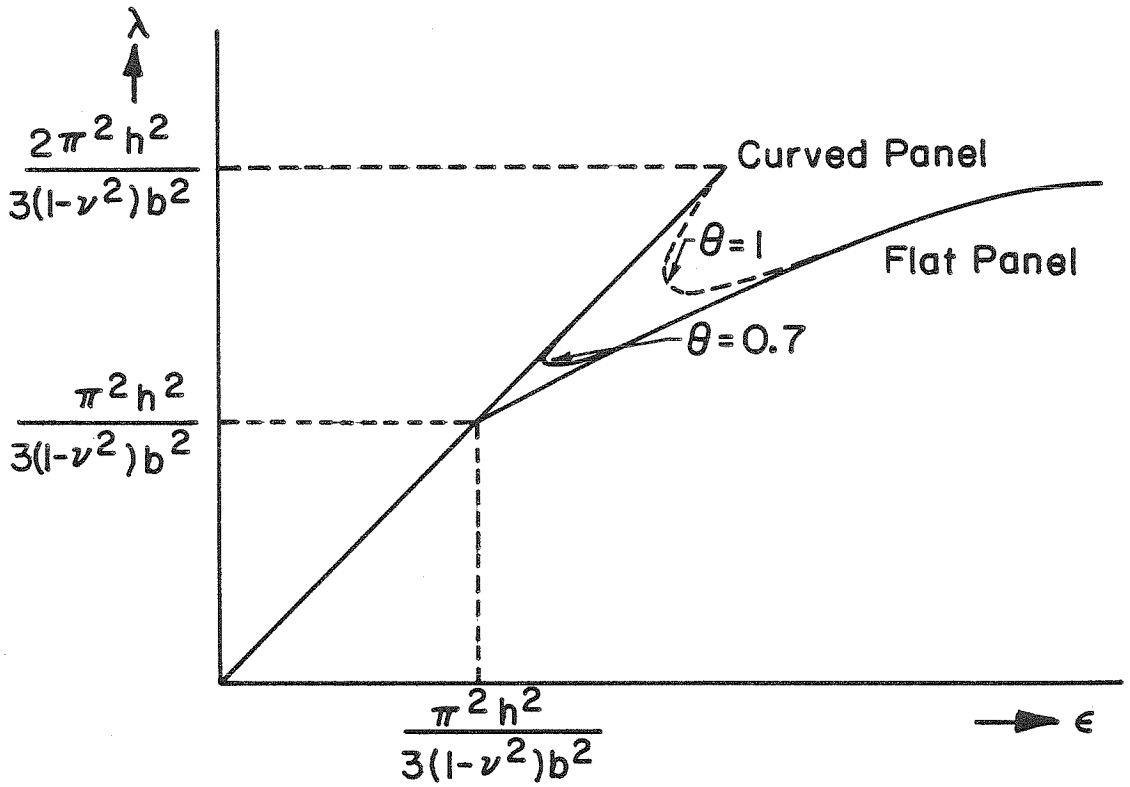

FIG. 36 CONJECTURED POST-BUCKLING CURVES IN ADVANCED STAGE FOR NARROW CYLINDRICAL PANELS